Monthly Notices of the ROYAL ASTRONOMICAL SOCIETY

MNRAS **502,** 5455–5470 (2021) doi:10.1093/mnras/stab345
Advance Access publication 2021 February 6

Distances to Galactic X-ray binaries with *Gaia* DR2

R. M. Arnason,[1]★ H. Papei ,[1] P. Barmby ,[1,2]★ A. Bahramian [3] and M. D. Gorski [1,4]

[1]*Department of Physics & Astronomy*
[2]*Institute for Earth and Space Exploration, University of Western Ontario, 1151 Richmond Street, London, ON N6A 3K7, Canada*
[3]*International Centre for Radio Astronomy Research, Curtin University, GPO Box U1987, Perth, WA 6845, Australia*
[4]*Department of Space, Earth & Environment, Astronomy and Plasma Physics, Chalmers University of Technology, SE-412 96 Gothenburg, Sweden*

Accepted 2021 February 2. Received 2021 February 2; in original form 2020 March 30

ABSTRACT

Precise and accurate measurements of distances to Galactic X-ray binaries (XRBs) reduce uncertainties in the determination of XRB physical parameters. We have cross-matched the XRB catalogues of Liu, van Paradijs & van den Heuvel to the results of *Gaia* Data Release 2. We identify 86 XRBs with a *Gaia* candidate counterpart, of which 32 are low-mass X-ray binaries (LMXBs) and 54 are high-mass X-ray binaries (HMXBs). Distances to *Gaia* candidate counterparts are, on average, consistent with those measured by *Hipparcos* and radio parallaxes. When compared to distances measured by *Gaia* candidate counterparts, distances measured using Type I X-ray bursts are systematically larger, suggesting that these bursts reach only 50 per cent of the Eddington limit. However, these results are strongly dependent on the prior assumptions used for estimating distance from the *Gaia* parallax measurements. Comparing positions of *Gaia* candidate counterparts for XRBs in our sample to positions of spiral arms in the Milky Way, we find that HMXBs exhibit mild preference for being closer to spiral arms; LMXBs exhibit mild preference for being closer to interarm regions. LMXBs do not exhibit any preference for leading or trailing their closest spiral arm. HMXBs exhibit a mild preference for trailing their closest spiral arm. The lack of a strong correlation between HMXBs and spiral arms may be explained by star formation occurring closer to the mid-point of the arms, or a time delay between star formation and HMXB formation manifesting as a spatial separation between HMXBs and the spiral arm where they formed.

Key words: parallaxes – Galaxy: structure – X-rays: binaries – X-rays: bursts.

1 INTRODUCTION

1.1 X-ray binaries

X-ray binaries (XRBs) are rare systems comprised of a main-sequence star in a close binary orbit with a neutron star (NS) or black hole (BH). The accretion of material from the main-sequence companion on to the compact object results in X-ray emission that dominates much of the point source population of the X-ray sky. Aside from the type of accretor, XRBs are principally categorized based on the mass of the companion. Binaries where the compact object accretes from the wind of a star >10 $M_\odot$ are classified as high-mass X-ray binaries (HMXBs), while those that accrete from the Roche lobe overflow of a <1 $M_\odot$ companion are known as low-mass X-ray binaries (LMXBs; van Paradijs 1998; Casares, Jonker & Israelian 2017). There are a handful of XRBs where the companion is of intermediate mass 1–3 $M_\odot$, but they are rare compared to the other two types of system. It is expected that many primordial intermediate-mass X-ray binaries have evolved to LMXBs in the present day through mass transfer (Podsiadlowski & Rappaport 2000).

XRBs are interesting extraterrestrial laboratories that permit the testing of our understanding of physical processes under extremes of gravity, rotation rate, pressure, temperature, and magnetic field strength. In addition, a number of interesting astrophysical phenomena can be studied through XRBs, such as wind physics, NS equation of state, and high-energy radiative processes. Aside from their value to these astrophysical questions, XRBs can also provide independent constraints on their formation environment on larger scales (Lehmer et al. 2010; Boroson, Kim & Fabbiano 2011; Zhang, Gilfanov & Bogdán 2012; Tremmel et al. 2013). LMXBs can act as independent tracers of stellar mass, since low-mass stars comprise the bulk of the stellar mass in a population (Gilfanov 2004). Additionally, LMXBs are preferentially found in areas of high stellar density, such as the globular clusters of the Galaxy and in the direction of the Galactic Centre, likely due to their formation by dynamical mechanisms (Clark 1975; Pooley et al. 2003; Muno et al. 2005; Verbunt & Lewin 2006; Degenaar et al. 2012). By contrast, the high-mass companions of HMXBs are short lived, so they are useful for tracing recent star formation in a long-term Galactic evolution context. Observations of nearby galaxies have suggested that the star formation rate (SFR) of a galaxy scales with both the number of HMXBs and their collective X-ray luminosity, albeit with a moderate dispersion (Grimm, Gilfanov & Sunyaev 2003; Mineo, Gilfanov & Sunyaev 2012). Finally, XRBs are one of the few ways to observe the high-mass end of the initial mass function in an evolved population, since isolated NSs and BHs are challenging to observe and study (Verbunt & Hut 1987; Verbunt 2003; Dabringhausen et al. 2012).

1.2 X-ray binaries and Galactic structure

Although field Milky Way XRBs can often be easier to study because of their close proximity (compared to XRBs in globular clusters or

★ E-mail: rarnaso@uwo.ca (RMA); pbarmby@uwo.ca (HP)

other galaxies), investigating the relationship between XRBs and galaxy parameters for the Milky Way is complicated. Our location within the disc of the Milky Way means that lines of sight where XRBs are expected to be more abundant tend to be heavily extincted.

XRBs tend to have a spatial distribution that is distinct from ordinary stars belonging to the same parent stellar population because the supernova that forms the compact object in an XRB system can impart a velocity kick to the system, often known as a 'natal' kick. This velocity kick has two effects: it gives the XRB system a peculiar velocity relative to Galactic rotation, and it can substantially displace the system (depending on XRB type) from the star-forming region where its progenitor formed (González Hernández et al. 2005; Dhawan et al. 2007). Repetto, Davies & Sigurdsson (2012) investigated how natal kicks at the birth of BH LMXBs are necessary to explain their observed distribution in the Milky Way, particularly the presence of LMXBs at significant (1 kpc) distances above the disc. They found that these kicks tend to be similar to those found for NSs, a property which has been interpreted as a consequence of the asymmetry of the supernova explosion (Janka 2013).

Naively, we expect that if HMXBs are correlated with star formation on a global scale, they should have a spatial correlation with the sites of star formation in the spiral arms. The shape and extent of the Milky Way's spiral arms is not easy to resolve compared to external galaxies observed face-on. Positions of the spiral arms themselves are typically inferred through the fitting of analytical models to an ensemble of observational tracers, including CO maps, H II regions, pulsars, masers, stellar kinematics, and dust emission (Vallée 2014). To date, investigations of the correlation between HMXBs and the spiral arms have been done using only two proxies of the spiral arms. Bodaghee et al. (2012) measured spatial cross-correlation between OB associations and HMXBs, finding that they have a characteristic offset of 0.4 ± 0.2 kpc, which is attributed to natal kicks received by HMXBs at their formation. However, by the same models they find no correlation between either OB associations or HMXBs and the spiral arms themselves, which is unexpected given that OB associations are expected to trace out the spiral arms (Brown et al. 1999). Coleiro & Chaty (2013) investigated the spatial relation between HMXBs and star-forming complexes (SFCs) finding that they are correlated on two characteristic scales: 0.3 ± 0.05 and 1.7 ± 0.3 kpc, which they interpret as the cluster size and cluster separation, respectively. They also derive a mean migration distance for HMXBs of roughly 0.1 pc and mean migration ages of around 50 Myr (depending on HMXB type) though they note that sample sizes are small and uncertainties are large. A large source of that uncertainty lies in the difficulty in determining distances to XRBs within the Milky Way.

1.3 X-ray binary distances

A principal reason for desiring accurate distances to XRBs in the Milky Way is that many of these XRBs can be studied in detail. With the exception of XRBs located in the direction of the Galactic Centre, in the Milky Way the population of XRBs can be studied to fainter X-ray luminosities, and identifications of a unique optical counterpart are more straightforward. Since individual XRBs are most easily studied in the Milky Way, our understanding of individual XRBs in other galaxies and their parameters as an ensemble population are affected by studies of nearby XRBs. Measuring the distance to individual XRBs accurately is important because the uncertainty on a number of desired properties in an XRB system can be limited by the uncertainty on distance. For example, measurements of distance can affect the inferred size of the accretor (i.e. NS radius), inferred mass of either component of the system (either the companion mass or the mass of the accreting NS/BH), inferred mass transfer rate, and other relevant accretion physics due to the inferred luminosity (Galloway et al. 2003; Jonker & Nelemans 2004; Nättilä et al. 2017; Steiner et al. 2018).

The principal difficulty in measuring distances to XRBs is that they lack a universal property or characteristic that would allow them to be used as a standard candle. XRBs are also extremely rare compared to ordinary stars, meaning that population-based methods of determining distances to objects, such as main-sequence fitting of a star cluster, cannot be used on XRB populations. Although one can use the main sequence of ordinary stars in a cluster to determine the distance to XRBs in that cluster, the rarity of XRBs means that constructing an 'XRB main sequence' is untenable. X-ray emission from the accretor that irradiates the companion may modify the expected emission at longer wavelengths, causing an excess in the bluer filters of the visible domain (Phillips, Shahbaz & Podsiadlowski 1999; Muñoz-Darias, Casares & Martínez-Pais 2005; Bozzo et al. 2018; Linares, Shahbaz & Casares 2018). Failing to account for these effects on the expected optical emission of an XRB may lead to incorrect estimates of distance from photometric methods. These effects are themselves modified by the mass transfer rate, accretion geometry, orbital phase, and accretion state of the system, meaning that they can change with time and may require simultaneous multiwavelength observations for distances to be usefully constrained.

A number of techniques have been used to constrain distance measurements of Milky Way XRBs. The most common of these is to measure a photometric distance by assuming that the emission is dominated by the companion at longer wavelengths. In general, this method is subject to substantial uncertainties, not only due to the contribution of the accretor, but also due to uncertainties in spectral classification and calibrating the absolute magnitude (Reig & Fabregat 2015). A small number of XRBs have had their distances determined via radio parallax or the proper motion of a launched jet (Hjellming & Johnston 1981; Bradshaw, Fomalont & Geldzahler 1999; Miller-Jones et al. 2009). This form of measurement provides relatively tight constraints on distance, but is possible only for objects that are sufficiently radio bright and moderately nearby.

An X-ray specific method of measuring distances is to use the observed flux from Type I X-ray bursts. These bursts occur when a sufficient amount of accreted material, mostly hydrogen, accumulates on the surface of an NS to trigger a thermonuclear runaway that produces a characteristic burst (Lewin, van Paradijs & Taam 1993). The burst is specifically the result of nuclear burning on the NS. A subset of these bursts have steady hydrogen burning followed by ignition of a helium layer beneath the hydrogen layer on the surface. The ignition of this helium layer produces a burst that is sufficient to lift the photosphere off the surface of the NS. These bursts are known as photospheric radius expansion (PRE) bursts, and the luminosity of the X-ray burst is expected to be at the Eddington luminosity during the expansion and contraction of the photosphere (Kuulkers et al. 2003). Since the Eddington limit is fixed for a particular accretor mass (and gas composition/opacity), this means that the mass, radius, and distance of an NS can be constrained by comparing the observed flux to the modelled Eddington luminosity for that object. (Strohmayer & Bildsten 2006; Bhattacharyya 2010). The use of X-ray bursts to infer distance was suggested not long after the detection of such bursts by early X-ray satellites. This relation has been calibrated using X-ray bursts observed in Galactic globular clusters (van Paradijs 1978, 1981; Verbunt, van Paradijs & Elson 1984) and applied to several Galactic XRBs that exhibit either PRE or PRE-like bursts (Basinska et al. 1984; Galloway et al. 2003;

Jonker et al. 2004). Evaluations of this method have shown that uncertainties around the modelling assumptions in this method can result in uncertainties in distance, NS mass, and NS radius (Galloway, Özel & Psaltis 2008b).

With the exception of Type I X-ray bursts, most of the distance-determination techniques require the identification of an optical/infrared counterpart to the X-ray source. Identification of a counterpart requires high spatial resolution and accurate determination of X-ray position. Existing catalogues of XRBs include sources that have not been redetected since their discovery prior to the era of high angular resolution telescopes, and as such have poorly determined positions that could have many candidate counterparts. The presence of interstellar extinction along particular lines of sight can interfere with the identification of optical counterparts for many XRB sources. Aside from studies of individual objects using telescopes such as the *Hubble Space Telescope*, the principal existing parallax survey of objects in the Milky Way was conducted by the *Hipparcos* satellite (Perryman et al. 1997). *Hipparcos* provides parallax for only $\sim 10^5$ sources, and has a fairly shallow limiting magnitude of 12. A handful of nearby XRBs have had their distances determined via *Hipparcos* parallax (see e.g. Chevalier & Ilovaisky 1998). *Hipparcos* data provide reliable measurements of distance within a few hundred parsecs of the Sun, which excludes (based on estimates using the other distance methods described above) the overwhelming majority of XRBs known in the Milky Way.

1.4 *Gaia* DR2 as a probe of XRB distances

The successor to *Hipparcos*, the *Gaia* satellite, was launched in 2013 and aims to have full five-parameter measurements (position, proper motion, parallaxes) for ∼1 billion stars and parallaxes accurate to 10 per cent for approximately 100 million sources by the end of its 5-yr mission (Gaia Collaboration 2016a). To date, there have been two full data releases of *Gaia* results and an early release of a third version (Gaia Collaboration 2016b, 2018, 2020). *Gaia* data release 2 (DR2), released in 2018 April and based on the first 22 months of data taken, contains over 1.3 billion sources that have full five-parameter measurements, an improvement of five orders of magnitude of *Hipparcos* for parallax measurements. Depending on the required uncertainties, *Gaia* DR2 contains measurements for objects to a limiting *G* magnitude of 17–21. So far, *Gaia* DR2 has already provided a wealth of information for studying populations in and nearby the Milky Way that deviate from the expected dynamics of ordinary stars in the Milky Way. For example, measurements of candidate hypervelocity stars using *Gaia* DR2 have shown that many of them are in fact bound to the Milky Way, but at least one object has an origin in the direction of the Magellanic Clouds, suggesting the presence of a supermassive BH in the Large Magellanic Cloud (Boubert et al. 2018; Erkal et al. 2019). Gandhi et al. (2019) searched for *Gaia* DR2 candidate counterparts for Galactic BH transients, finding that distances from *Gaia* counterparts generally agreed with prior distance estimates. Notably, they found that the BH BW Cir has a *Gaia* distance of $\sim 0.6 \pm 0.2$ kpc, making it the closest dynamically confirmed transient BH, although this distance is difficult to reconcile with interpretations of the properties of the donor star.

In this work, we seek to expand the use of *Gaia* to measure distances to XRBs and assess the accuracy of pre-*Gaia* distance measurements. We include not only binaries with BHs/BH candidates but also NS/NS candidate binaries and those with no clear identification of accretor type. Given that XRBs are expected to deviate from the Milky Way's stellar distribution in subtle to dramatic ways, *Gaia* DR2 offers a unique chance to create a sample of XRBs whose distances are determined by a uniform method, as compared with the heterogeneous mix of methods used for XRB distance determination whose accuracies, systematics, and model dependences may vary greatly. It also offers an opportunity to calibrate alternative methods of measuring distance for use in the general case where parallax measurements are not available. *Gaia* DR2 measurements are subject to several known systematic effects, including centroid wobble caused by unresolved stellar companions (Belokurov et al. 2020) and variation in the parallax zero-point with source colour and spatial location (Arenou et al. 2018; Lindegren et al. 2018). However, the widespread use of *Gaia* data means that these systematics have been investigated and characterized by many different groups (e.g. Chan & Bovy 2020, summarize many determinations of the zero-point offset). Uncertainties and systematics are, in general, more poorly understood for the one-off distance measurements available in the literature for many XRBs.

2 SAMPLE AND METHODS

Cross-matching XRBs to *Gaia* requires input catalogue(s) of known XRBs and XRB candidates. To date, the most comprehensive catalogues of XRBs in the Milky Way are the catalogues of high-mass and low-mass XRBs by Liu et al. (2006, 2007). In general, properties of these XRBs (including positional uncertainties) are compiled using the best/most recent (at the time of catalogue creation) observations of these objects. These catalogues are assembled from published observations taken with a variety of X-ray telescopes, including *Uhuru*, *Einstein*, *ROSAT*, *RXTE*, *Chandra*, and *XMM–Newton*. As such, the specific X-ray energies sampled, sensitivities, and coverage of these catalogues are non-uniform. Since the most recent updates to these catalogues were in 2006 and 2007, they do not include a number of Galactic XRB candidates discovered since then. However, an advantage of these catalogues is that many of these objects have been studied in detail, especially those with identified counterparts. This implies that the expected number of non-XRB contaminants should be low.

2.1 XRB sample

In order to assemble a sample of XRBs for *Gaia* counterpart matching, we combine the Liu et al. (2006, 2007) catalogues of Galactic HMXBs and LMXBs. Although the most recent revision of these catalogues is now over a decade old, they still represent the most complete sample in the literature. In total, these catalogues contain 301 XRBs or XRB candidates. We have removed two objects from the Liu catalogues: 1H 0556+286, and 1H 1255−567 (Mu-2 Cru), on the basis that they appear to have been misclassified as HMXBs and are in fact ordinary stars (Berghoefer, Schmitt & Cassinelli 1996; Torrejón & Orr 2001). The majority of the objects have positional accuracies (equivalent 90 per cent confidence) ∼1 arcsec or better, typically through identification of an optical counterpart or high-resolution X-ray observation. However, a number of the candidate objects in these catalogues have poorly determined positions, especially those that have not been reobserved since the beginning of the *Chandra* era. We assume that long-wavelength counterparts identified in the catalogues are true counterparts to the LMXB/HMXB or LMXB/HMXB candidates. In order to feasibly attempt to identify *Gaia* counterparts, we select only objects whose positional accuracy is quoted in the catalogues as better than <10 arcsec, which provides a sample of 220 XRBs, of which 136 are LMXBs and 84 are HMXBs.

2.2 Published distance estimates

Distances to XRBs are estimated using many different methods and a goal of this work is to evaluate the quality of these methods (see also Jonker & Nelemans 2004; Thévenin et al. 2017). The Liu et al. (2006, 2007) catalogues provide distance estimates in the notes to the main catalogue files. We include the previous distances and original references, as well as an indication of the distance measurement method in Tables 1 and 2, for LMXBs and HMXBs matched to *Gaia* sources, respectively. In some cases, only a distance range is quoted in the Liu et al. catalogues and we give the centre of this range. In cases where an upper or lower limit was given, we quote that number as the distance. 15 of the XRBs with *Gaia* candidate counterparts (Section 2.4) had no previous distance measurement as of the Liu catalogues. The results of our literature search for these objects are discussed in Appendix A; we found published distances for 10 of these 15 objects. We also updated distances for 15 additional objects that had more recently published distances than those given in the Liu catalogues.

The majority of the objects in our sample have distances measured through photometry of the companion, using measured apparent magnitude and extinction with an assumed absolute magnitude based on modelling. Many XRBs with an NS have had their distance measured using Type I X-ray bursts. Aside from these categories, there are also a handful of objects with *Hipparcos* or radio parallaxes, and a variety of other methods for individual objects. We use the following labels for different distance methods:

(i) Phot: photometric distance using apparent magnitude, extinction, and assumed absolute magnitude of companion.
(ii) SEDfit: broad-band SED is fit to an assumed model of the companion star/accretion disc with distance as a fitted parameter.
(iii) A_V: distance measured using extinction models/Galactic column density.
(iv) jetPM: distance measured using jet proper motion.
(v) Cluster: distance is assumed to be that of an associated cluster/OB association.
(vi) Burst: X-ray burst is used as a standard candle to obtain distance.
(vii) VLBAPLX/VLBIPLX: parallax measured using radio interferometery
(viii) Kin: distance inferred from the kinematics of associated H II regions.
(ix) HipPLX: distance measured using parallax from the *Hipparcos* satellite.
(x) Unknown: no previous distance measurement.

In the literature, uncertainties on distances to XRBs are reported in different ways, including making approximations with no quoted uncertainties. As such, in this work we do not attempt to track the uncertainties associated with previous measurements, except for a handful of cases. In particular, we expect that distances from a radio parallax (VLBI or VLBA) measurement should be more precise than those from *Gaia* DR2, and *Gaia* DR2 distances should agree with parallaxes measured with the *Hipparcos* satellite. In general, we expect that the distance to *Gaia* candidate counterparts is more reliable and that the *Gaia* DR2 methodology and systematics are, when taken as a whole, better understood than for the heterogeneous ensemble of other methods.

2.3 Cross-matching

We searched for counterparts to our XRB sample by cross-matching with the *Gaia* DR2 public release. Initially, we collected all potential counterparts with a tolerance of <10 arcsec and then refined the matches to only include counterparts whose angular separation was less than the quoted positional uncertainty for each individual object. As per the catalogue description, any object that does not have a quoted positional uncertainty is assumed to be accurate to $\sim$1 arcsec or better (Liu et al. 2006, 2007). We have chosen the conservative case of a $\sim$1 arcsec positional uncertainty for these objects. In the case that an object had asymmetric positional uncertainties in right ascension versus declination, we conservatively chose the maximum of these two. With this refinement, 99 XRBs from the Liu catalogues have at least one candidate *Gaia* counterpart. In total, we find 126 potential counterparts for the Liu XRBs. Most objects have only one counterpart, while a handful (those with more poorly determined positional accuracy) return two or more potential counterparts.

We further refined our sample of potential XRB counterparts by considering the probability that each *Gaia* source is aligned with the position of the XRB by chance alone. To estimate probability of our X-ray sources matching a random *Gaia* source, we picked 5000 random coordinates within 0.1 deg of each X-ray source and cross-matched these random realizations against the *Gaia* catalogue to identify the closest real *Gaia* source to each random pair of coordinates and measured the angular distance between each random pair of coordinates and the closest real *Gaia* source to that pair. The distribution of these distances in the vicinity of each X-ray source (for which these random samples were generated and cross-matched against Gaia) is directly proportional to the probability of chance overlap between a source in the *Gaia* catalogue and any random pair of coordinates (informed partially by the density of *Gaia* catalogue in the vicinity of each X-ray source). We approximated the probability of a random match by the fraction of random points which are located within a distance of a *Gaia* source equal to the separation between the X-ray source and the candidate *Gaia* counterpart. After removing the counterparts with a probability of chance overlap greater than 10 per cent, we obtain 88 *Gaia* candidate counterparts to the Liu XRB sample, most of which have reported parallaxes.[1] A complete list of Liu et al. (2006, 2007) catalogue sources that were excluded from the final sample and the step at which they were excluded is found in the online supporting information. At this level, only two objects have more than one potential *Gaia* counterpart: AX J1639.0−4642 and SAX J1711.6−3808. Each of these objects has one potential counterpart with a parallax, and one without. In the case of AX J1639.0−4642, the counterpart with parallax is the more probable and we retain that parallax for our analysis. The opposite is true for SAX J1711.6−3808; as for other objects where the *Gaia* counterpart does not have a parallax, it does not feature in our further analysis. We searched the literature for more recent distance determinations and any changes to the XRB-type classification for all of the 88 matches. We found no strong evidence to reclassify individual source types but did find a few additional published distances (see Appendix A).

Before proceeding, we consider the potential biases of our sample compared to the unmatched sample. HMXBs have more luminous main-sequence components and unsurprisingly are more likely to have a counterpart than LMXBs: there are 187 LMXBs and 114 HMXBs in the Liu catalogues, but we find only 33 and 55 *Gaia* candidate counterparts to LMXBs and HMXBs, respectively (these numbers each decrease by one after removing the extra candidate

[1]Except for 2S 0053+604 (see Appendix A), the counterparts without parallaxes are faint ($18.8 < G < 21.0$) and the lack of parallax measurement is consistent with the distributions given by Gaia Collaboration (2018).

Table 1. Properties of *Gaia* candidate counterparts to Galactic LMXBs.

Names	RA	Dec.	$P_{\rm interloper}$	*Gaia* DR2 ID	$\theta_{\rm sep}$ (arcmin)	$m_{\rm G,mean}$ (mag)	GOF	$d_{\rm Gaia}$ (kpc)	$d_{\rm prev}$ (kpc)	$d_{\rm prev}$ type	$d_{\rm prev}$ ref.
GRO J0422+32/V518 Per	04 21 42.790	+32 54 27.10	0.0100	172650748928103552	0.86	20.85 ± 0.05	4.4	···	2.49	SED fit	Gelino & Harrison (2003)
Swift J061223.0+701243.9/-	06 12 22.600	+70 12 43.40	0.0001	1107229825742589696	0.29	21.00 ± 0.06	1.6	···	···	···	···
4U 0614+091/V1055 Ori	06 17 07.400	+09 08 13.60	0.0051	3328832132393159296	0.65	18.56 ± 0.02	1.4	$3.3^{+1.3}_{-2.4}$	3.0	Burst	Brandt et al. (1992)
1A 0620−00/V616 Mon	06 22 44.503	−00 20 44.72	0.0070	3118721026600835328	0.73	17.52 ± 0.01	3.0	$1.6^{+0.4}_{-0.7}$	1.06	Phot	Cantrell et al. (2010)
4U 0919−54/∗X	09 20 26.950	−55 12 24.70	0.0009	5310395631783100800	0.1	20.73 ± 0.02	3.0	···	5.4	Burst	in't Zand et al. (2005)
GS 1124−684/GU Mus	11 26 26.700	−68 40 32.60	0.0209	5234956524083372544	0.64	19.57 ± 0.01	0.4	$2.3^{+1.1}_{-3.1}$	5.9	SED fit	Gelino (2001)
1A 1246−588/∗X	12 49 39.364	−59 05 14.68	0.0002	6059778089610749440	0.04	20.495 ± 0.008	1.2	$2.0^{+1.2}_{-2.4}$	5.0	Burst	Bassa et al. (2006)
4U 1456−32/V822 Cen	14 58 22.000	−31 40 08.00	0.0077	6205715168442046592	0.96	17.865 ± 0.005	0.7	$2.1^{+0.6}_{-1.2}$	1.3	Burst	Kaluzienski, Holt & Swank (1980)
3A 1516−569/BR Cir	15 20 40.900	−57 10 01.00	0.0763	5883218164517055488	0.87	17.92 ± 0.02	11.5	$6.2^{+2.0}_{-2.9}$	9.2	Burst	Jonker & Nelemans (2004)
1E 1603.6+2600/UW CrB	16 05 45.820	+25 51 45.10	0.0018	1315375795016730880	0.75	19.67 ± 0.01	2.4	$2.1^{+0.7}_{-1.2}$	6.0	Burst	Hakala et al. (2005)
H 1617−155/V818 Sco	16 19 55.070	−15 38 24.80	0.0001	4328198145165324800	0.22	12.48 ± 0.02	9.4	$2.13^{+0.21}_{-0.26}$	2.8	VLBAPLX	Bradshaw et al. (1999)
4U 1636−536/V801 Ara	16 40 55.500	−53 45 05.00	0.0819	5930753870442684544	0.87	18.27 ± 0.02	0.5	$4.4^{+1.6}_{-3.1}$	6.0	Burst	Galloway et al. (2008a)
GRO J1655−40/V1033 Sco	16 54 00.137	−39 50 44.90	0.0022	5969790961312131456	0.15	16.224 ± 0.006	4.0	$3.3^{+0.7}_{-1.1}$	3.2	Jet PM	Hjellming & Rupen (1995)
2A 1655+353/HZ Her	16 57 49.830	+35 20 32.60	<0.0001	1338822021487330304	0.26	13.61 ± 0.02	10.4	$5.0^{+0.6}_{-0.7}$	6.6	SED fit	Reynolds et al. (1997)
MXB 1659−298/V2134 Oph	17 02 06.500	−29 56 44.10	0.0517	6029391608332996224	0.48	19.44 ± 0.04	0.1	···	10.0	Burst	Muno et al. (2001)
4U 1700+24/HD 154791	17 06 34.520	+23 58 18.60	<0.0001	4571810378118789760	0.09	6.743 ± 0.001	20.0	$0.536^{+0.009}_{-0.009}$	0.42	Phot	Masetti et al. (2002)
3A 1702−363/V1101 Sco	17 05 44.500	−36 25 23.00	0.0011	5976748056765619328	0.11	17.757 ± 0.008	−0.0	$4.9^{+1.7}_{-2.9}$	9.2	Unclear	van Paradijs & White (1995)
SAX J1711.6−3808/-	17 11 37.100	−38 07 05.70	0.0299	5973177495780065664	0.99	21.05 ± 0.02	0.5	···	···	···	···
4U 1724−307/Ter 2	17 27 33.300	−30 48 07.00	0.0347	4058208396397618688	0.34	18.20 ± 0.02	17.2	$6.6^{+2.8}_{-4}$	9.5	Cluster	Kuulkers et al. (2003)
3A 1728−247/V2116 Oph	17 32 02.160	−24 44 44.00	0.0012	4110236324513030656	0.15	15.860 ± 0.009	20.0	$7.6^{+2.8}_{-4}$	4.5	Phot	Chakrabarty & Roche (1997)
4U 1735−444/V926 Sco	17 38 58.300	−44 27 00.00	0.0742	5955379701104735104	0.96	17.77 ± 0.01	1.0	$5.6^{+2.1}_{-4}$	9.1	Burst	Augusteijn et al. (1998)
SLX 1737−282/-	17 40 43.000	−28 18 11.90	0.0816	4060255373456473984	0.69	14.602 ± 0.003	47.8	$4.5^{+2.1}_{-4}$	6.5	Burst	in't Zand et al. (2002)
EXO 1747−214/star	17 50 24.520	−21 25 19.90	0.0067	4118590585673834624	0.17	20.24 ± 0.03	3.0	···	11.0	Burst	Tomsick, Gelino & Kaaret (2005)
Swift J1753.5−0127/-	17 53 28.290	−01 27 06.22	<0.0001	4178766135477201408	0.04	16.698 ± 0.009	0.6	$5.6^{+1.8}_{-2.8}$	6.0	A_V	Cadolle Bel et al. (2007)
4U 1755−33/V4134 Sgr	17 58 40.000	−33 48 27.00	0.0277	4042473487415175168	0.35	19.500 ± 0.007	3.7	···	6.5	Phot	Wachter & Smale (1998)
2A 1822−371/V691 CrA	18 25 46.800	−37 06 19.00	0.0186	6728016172687965568	0.52	15.53 ± 0.02	3.7	$6.1^{+1.6}_{-2.7}$	2.5	SED fit	Mason & Cordova (1982)
HETE J1900.1−2455/star	19 00 08.650	−24 55 13.70	0.0007	4074363039644919936	0.17	18.10 ± 0.01	−0.1	$3.5^{+1.7}_{-3.5}$	5.0	Burst	Kawai & Suzuki (2005)
4U 1908+005/V1333 Aql	19 11 16.000	+00 35 06.00	0.0638	4264296556603631872	0.87	18.901 ± 0.004	2.4	$3.0^{+1.3}_{-2.6}$	5.2	Burst	Jonker & Nelemans (2004)
4U 1916−05/V1405 Aql	19 18 47.870	−05 14 17.09	0.0066	4211396994895217152	0.37	20.92 ± 0.03	0.6	···	8.9	Burst	Galloway et al. (2008a)
3A 1954+319/star	19 55 42.330	+32 05 49.10	0.0014	2034031438383765760	0.12	8.370 ± 0.002	23.6	$3.3^{+0.6}_{-1.0}$	1.7	Phot	Masetti et al. (2006b)
GS 2023+338/V404 Cyg	20 24 03.830	+33 52 02.200	0.0058	2056188620566335360	0.24	17.19 ± 0.01	4.0	$2.1^{+0.4}_{-0.6}$	2.39	VLBIPLX	Miller-Jones et al. (2009)
4U 2129+47/V1727 Cyg	21 31 26.200	+47 17 24.00	0.0106	1978241050130301312	0.53	17.600 ± 0.001	1.9	$1.75^{+0.26}_{-0.4}$	6.3	Phot	Cowley & Schmidtke (1990)

Note. First name in each column indicates the first name in the catalogue, while the second name indicates the name of the optical counterpart (if any). Optical counterparts that have numbers/letters following a ∗ refers to the corresponding object on the finding chart as described in the Liu catalogues. Optical counterparts with the name 'star' do not have a labelled object on their corresponding finding chart. $\theta_{\rm sep}$ indicates the separation between the candidate *Gaia* counterpart and the quoted position of the XRB in Liu et al. (2006, 2007). GOF is the *Gaia* DR2 goodness-of-fit statistic `astrometric_gof_al`.

Table 2. Properties of *Gaia* candidate counterparts to Galactic HMXBs.

Names	RA	Dec.	$P_{\rm interloper}$	*Gaia* DR2 ID	$\theta_{\rm sep}$ (arcmin)	$m_{\rm G,mean}$ (mag)	GOF	$d_{\rm Gaia}$ (kpc)	$d_{\rm prev}$ (kpc)	$d_{\rm prev}$ type	$d_{\rm prev}$ ref.
2S 0053+604/gamma Ca	00 56 42.50	+60 43 00.0	0.0041	426558460877467776	0.66	1.82 ± 0.01	190.5	...	0.19	HipPLX	Perryman et al. (1997)
2S 0114+650/V662 Cas	01 18 02.70	+65 17 30.0	0.0005	524924310153249920	0.17	10.520 ± 0.001	5.5	$6.6^{+1.1}_{-1.6}$	7.2	Phot	Reig et al. (1996)
RX J0146.9+6121/LS I + 61 235	01 47 00.20	+61 21 23.7	0.0001	511220031584305536	0.1	11.210 ± 0.002	19.3	$2.50^{+0.18}_{-0.21}$	2.3	Phot	Coe et al. (1993)
IGR J01583+6713/-	01 58 18.44	+67 13 23.5	0.0009	518990967445248256	0.3	13.7000 ± 0.0007	−1.1	$7.4^{+0.8}_{-1.1}$	6.4	Phot	Masetti et al. (2006c)
1E 0236.6+6100/LS I + 61 303	02 40 31.70	+61 13 46.0	0.0031	465645515129855872	0.48	10.390 ± 0.001	3.3	$2.45^{+0.21}_{-0.26}$	2.4	Kin	...
V 0332+53/BQ Cam	03 34 59.90	+53 10 24.0	0.0025	444752973131169664	0.71	14.220 ± 0.002	8.6	$5.1^{+0.8}_{-1.0}$	7.0	Phot	Negueruela et al. (1999)
RX J0440.9+4431/LS V + 44 17	04 40 59.30	+44 31 49.0	0.0014	252878401557369088	0.41	10.430 ± 0.001	−0.0	$3.2^{+0.5}_{-0.6}$	3.2	Phot	Motch et al. (1997)
EXO 051910+3737.7/V420 Aur	05 22 35.20	+37 40 34.0	0.0025	184497471323752064	0.52	7.220 ± 0.001	11.8	$1.29^{+0.09}_{-0.10}$	1.7	Phot	Polcaro et al. (1990)
1A 0535+262/V725 Tau	05 38 54.60	+26 18 57.0	0.0011	3441207615229815040	0.37	8.680 ± 0.007	5.6	$2.13^{+0.21}_{-0.26}$	2.45	Phot	Steele et al. (1998), Lyuty & Zaĭtseva (2000)
IGR J06074+2205/-	06 07 26.60	+22 05 48.3	0.0039	3423526544838563328	0.57	12.180 ± 0.001	3.1	$5.5^{+1.0}_{-1.5}$	4.5	Phot	Reig, Zezas & Gkouvelis (2010)
SAX J0635.2+0533/-	06 35 18.29	+05 33 06.3	<0.0001	3131755947406031104	0.15	12.510 ± 0.006	0.7	$5.7^{+1.3}_{-2.0}$	3.75	Phot	Kaaret et al. (1999)
XTE J0658−073/[M81] I-33	06 58 17.30	−07 12 35.3	0.0004	3052677318793446016	0.2	12.030 ± 0.003	4.1	$5.1^{+0.9}_{-1.4}$	3.9	Phot	McBride et al. (2006)
3A 0726−260/V441 Pup	07 28 53.60	−26 06 29.0	0.0019	5613494119544761088	0.3	11.620 ± 0.003	4.5	$9.5^{+2.1}_{-3.1}$	5.35	Phot	Corbet & Mason (1984), Negueruela et al. (1996)
1H 0739−529/HD 63666	07 47 23.60	−53 19 57.0	0.0005	5489434710755238400	0.22	7.5200 ± 0.0004	21.0	$0.643^{+0.017}_{-0.018}$	0.52	HipPLX	Chevalier & Ilovaisky (1998)
4U 0900−40/HD 77581	09 02 06.90	−40 33 17.0	0.0044	5620657678322625920	0.46	6.720 ± 0.002	9.6	$2.42^{+0.16}_{-0.19}$	1.9	Phot	Sadakane et al. (1985)
GRO J1008−57/star	10 09 46.90	−58 17 35.5	0.0052	5258414192353423360	0.52	13.900 ± 0.001	10.8	$3.6^{+0.4}_{-0.5}$	5.0	Phot	Coe et al. (1994)
1A 1118−615/Hen 3-640	11 20 57.20	−61 55 00.0	0.0055	5336957010898124160	0.25	11.6000 ± 0.0005	4.7	$2.93^{+0.22}_{-0.26}$	5.0	Phot	Janot-Pacheco, Ilovaisky & Chevalier (1981)
4U 1119−603/V779 Cen	11 21 15.10	−60 37 25.5	0.0021	5337498593446516480	0.14	12.890 ± 0.003	8.2	$6.4^{+1.0}_{-1.4}$	9.0	Phot	Krzeminski (1974), Hutchings et al. (1979)
IGR J11215−5952/HD 306414	11 21 46.81	−59 51 47.9	0.0017	5339047221168787712	0.12	9.760 ± 0.001	6.3	$6.5^{+1.1}_{-1.5}$	6.2	Phot	Masetti et al. (2006a)
IGR J11435−6109/-	11 44 10.70	−61 07 02.0	0.0363	5335022901224296064	0.64	13.000 ± 0.002	52.8	$3.9^{+1.1}_{-1.8}$	8.6	Phot	Masetti et al. (2009)
2S 1145−619/V801 Cen	11 48 00.00	−62 12 25.0	0.0023	5334823859608495104	0.18	8.630 ± 0.002	7.1	$2.23^{+0.16}_{-0.19}$	3.1	Phot	Stevens et al. (1997)
1E 1145.1−6141/V830 Cen	11 47 28.60	−61 57 14.0	0.0594	5334851450481641088	0.64	12.280 ± 0.001	6.6	$9.1^{+1.6}_{-2.2}$	8.0	Phot	Ilovaisky, Chevalier & Motch (1982)
4U 1223−624/BP Cru ?	12 26 37.60	−62 46 13.0	0.0075	6054569565614460800	0.37	9.760 ± 0.001	12.6	$3.5^{+0.4}_{-0.5}$	4.1	Phot	Leahy (2002)
1H 1249−637/HD 110432	12 42 50.30	−63 03 31.0	0.0037	6055103928246312960	0.24	5.120 ± 0.002	76.4	$0.416^{+0.021}_{-0.023}$	0.392	A_V	Megier et al. (2009)
1H 1253−761/HD 109857	12 39 14.60	−75 22 14.0	0.0003	5837600152935767680	0.16	6.5200 ± 0.0004	22.3	$0.2117^{+0.0014}_{-0.0014}$	0.24	HipPLX	Chevalier & Ilovaisky (1998)
4U 1258−61/V850 Cen	13 01 17.10	−61 36 07.0	0.0005	5863533199843070208	0.36	12.650 ± 0.003	16.0	$2.01^{+0.13}_{-0.15}$	2.4	Phot	Parkes, Murdin & Mason (1980)
2RXP J130159.6−635806/-	13 01 58.70	−63 58 09.0	0.0029	5862285700835092352	0.22	17.340 ± 0.001	6.7	$5.5^{+1.7}_{-2.8}$	5.5	Phot	Chernyakova et al. (2005)
2S 1417−624/∗7	14 21 12.90	−62 41 54.0	0.0995	5854175187681966464	0.81	20.490 ± 0.006	0.6	$3.8^{+1.7}_{-2.7}$	6.2	Phot	Grindlay, Petro & McClintock (1984)
4U 1538−52/QV Nor	15 42 23.30	−52 23 10.0	0.0267	5886085557746480000	0.72	13.190 ± 0.001	13.6	$6.6^{+1.4}_{-2.1}$	4.5	Phot	Clark (2004), Reynolds, Bell & Hilditch (1992)
1H 1555−552/HD 141926	15 54 21.80	−55 19 45.0	0.0610	5884544931471259136	0.74	8.680 ± 0.001	4.3	$1.35^{+0.08}_{-0.09}$	0.96	...	Grillo et al. (1992)
IGR J16318−4848/∗1	16 31 48.31	−48 49 00.7	0.0002	5940777877435137024	0.04	17.170 ± 0.002	32.4	$5.2^{+1.8}_{-2.7}$	0.9	SED fit	Filliatre & Chaty (2004)
AX J1639.0−4642/-	16 39 05.40	−46 42 14.0	0.0149	5942638074996489088	0.4	19.800 ± 0.006	7.3	$4.0^{+1.7}_{-2.6}$	...	...	...
IGR J16465−4507/-	16 46 35.26	−45 07 04.5	0.0008	5943246345430928512	0.11	13.510 ± 0.001	9.0	$2.70^{+0.35}_{-0.5}$	12.5	Phot	Smith (2004)
IGR J16479−4514/-	16 48 07.00	−45 12 05.8	0.0724	5940244030149933696	1.29	19.580 ± 0.005	3.5	$2.8^{+1.4}_{-2.5}$	4.45	Phot	Coley, Corbet & Krimm (2015)
4U 1700−37/HD 153919	17 03 56.80	−37 50 39.0	0.0154	5976382915813535232	0.33	6.400 ± 0.001	12.9	$1.75^{+0.19}_{-0.23}$	2.12	A_V	Megier et al. (2009)
XTE J1739−302/-	17 39 11.58	−30 20 37.6	0.0039	4056922105185686784	0.4	12.670 ± 0.001	34.1	$5.3^{+2.1}_{-4}$	2.3	Phot	Negueruela et al. (2006)
IGR J17544−2619/∗C1	17 54 25.28	−26 19 52.6	0.0006	4063908810076415872	0.1	11.670 ± 0.001	9.5	$2.66^{+0.33}_{-0.4}$	3.2	Phot	Pellizza, Chaty & Negueruela (2006)
SAX J1819.3−2525/V4641 Sgr	18 19 21.48	−25 25 36.0	0.0168	4053096217067937664	0.28	18.82 ± 0.02	3.2	...	6.2	SED fit	MacDonald et al. (2014)

Table 2 – *continued*

Names	RA	Dec.	$P_{\rm interloper}$	*Gaia* DR2 ID	$\theta_{\rm sep}$ (arcmin)	$m_{\rm G,mean}$ (mag)	GOF	$d_{\rm Gaia}$ (kpc)	$d_{\rm prev}$ (kpc)	$d_{\rm prev}$ type	$d_{\rm prev}$ ref.
RX J1826.2−1450/LS 5039	18 26 15.06	−14 50 54.3	0.0004	4104196427943626624	0.08	10.8000 ± 0.0004	−2.6	$1.96^{+0.19}_{-0.23}$	2.5	Phot	Casares et al. (2005)
AX J1841.0−0536/-	18 41 00.43	−05 35 46.5	0.0017	4256500538116700160	0.09	12.940 ± 0.003	34.3	$7.6^{+2.2}_{-3.1}$	10.0	A_V	Bamba et al. (2001)
XTE J1901+014/star	19 01 39.90	+01 26 39.2	0.0045	4268294763113217152	0.6	19.450 ± 0.007	0.2	$2.2^{+1.1}_{-2.2}$	…	…	…
XTE J1906+09/star	19 04 47.48	+09 02 41.8	0.0014	4310649149314811776	0.23	19.73 ± 0.01	6.8	$2.8^{+1.4}_{-2.3}$	10.0	A_V	Marsden et al. (1998)
3A 1909+048/SS 433	19 11 49.60	+04 58 58.0	0.0102	4293406612283985024	0.56	12.63 ± 0.02	18.1	$3.8^{+0.8}_{-1.1}$	5.5	Jet PM	Hjellming & Johnston (1981)
4U 1909+07/∗A	19 10 48.20	+07 35 52.3	0.0028	4306419980916246656	0.62	20.170 ± 0.008	10.6	$2.6^{+1.3}_{-2.3}$	7.0	A_V	Wen, Remillard & Bradt (2000)
IGR J19140+0951/-	19 14 04.20	+09 52 58.3	0.0056	4309253392325650176	0.41	18.200 ± 0.006	13.7	$2.8^{+1.3}_{-2.3}$	3.6	Phot	Torrejón et al. (2010)
1H 1936+541/DM + 53 2262	19 32 52.30	+53 52 45.0	0.0009	2136886799749672320	0.48	10.370 ± 0.002	23.2	$3.3^{+0.4}_{-0.5}$	…	…	…
XTE J1946+274/∗A	19 45 39.30	+27 21 55.4	0.0422	2028089540103670144	0.76	15.7100 ± 0.0007	6.8	$12.6^{+2.9}_{-4}$	9.5	SED fit	Wilson et al. (2003)
KS 1947+300/∗3	19 49 30.50	+30 12 24.0	0.0359	2031938140034489344	0.57	20.48 ± 0.01	−0.0	$3.1^{+2.0}_{-3.5}$	9.5	Pulsar	Tsygankov & Lutovinov (2005)
4U 1956+35/HD 226868	19 58 21.70	+35 12 06.0	0.0051	2059383668236814720	0.37	8.5200 ± 0.0008	3.6	$2.23^{+0.15}_{-0.18}$	1.86	VLBAPLX	Reid et al. ()
EXO 2030+375/∗2	20 32 15.20	+37 38 15.0	0.0116	2063791369815322752	0.9	16.910 ± 0.003	13.5	$3.6^{+0.9}_{-1.3}$	7.1	A_V	Wilson et al. (2002)
RX J2030.5+4751/SAO 49725	20 30 30.80	+47 51 51.0	0.0125	2083644392294059520	0.54	9.0300 ± 0.0006	9.1	$2.49^{+0.16}_{-0.19}$	2.2	Phot	Motch et al. (1997)
GRO J2058+42/star	20 58 47.50	+41 46 37.0	0.0048	2065653598916388352	0.45	14.190 ± 0.005	−0.3	$8.0^{+0.9}_{-1.2}$	9.0	…	Reig et al. (2005)
1H 2202+501/BD + 49 3718	22 01 38.20	+50 10 05.0	0.0029	1979911002134040960	0.37	9.3000 ± 0.0004	15.4	$1.16^{+0.05}_{-0.05}$	0.7	HipPLX	Chevalier & Ilovaisky (1998)
4U 2206+543/BD + 53 2790	22 07 56.20	+54 31 06.0	0.0086	2005653524280214400	0.52	9.7400 ± 0.0007	8.5	$3.34^{+0.32}_{-0.4}$	2.6	Phot	Blay et al. (2006)

Note. First name in each column indicates the first name in the catalogue, while the second name indicates the name of the optical counterpart (if any). Optical counterparts that have numbers/letters following a ∗ refers to the corresponding object on the finding chart as described in the Liu catalogues. Optical counterparts with the name 'star' do not have a labelled object on their corresponding finding chart. $\theta_{\rm sep}$ indicates the separation between the candidate *Gaia* counterpart and the quoted position of the XRB in Liu et al. (2006, 2007). GOF is the *Gaia* DR2 goodness-of-fit statistic `astrometric_gof_al`.

counterparts as described above). Our counterpart matching is also more sensitive to objects that are away from the Galactic Centre and away from the Galactic plane – the fraction of objects in the Liu catalogue that have a *Gaia* candidate counterpart is higher in those directions.

2.4 Distances and final sample

To obtain the distance for each counterpart, we match the *Gaia* source ID to the catalogue of Bailer-Jones et al. (2018), which uses a Bayesian method to infer distances. In this work, we quote distance uncertainties as the 1σ bounds on the posterior probability density function for distance. In general, this function is asymmetric about the peak value, so we have asymmetric error bars. The prior of this Bayesian method models the Galactic stellar density as an exponential disc, so the particular distance prior assumed for each object depends on that object's position in Galactic coordinates. For ordinary stars, information such as line-of-sight extinction, measured $T_{\rm eff}$, and magnitude/colours in the *Gaia* filters can provide additional distance constraints. However, for XRBs we prefer the position-plus-parallax-only method used by Bailer-Jones et al. (2018), since modelling the expected value of the additional other parameters in an XRB system is more complex than for an individual star or ordinary binary.

Since LMXBs do not follow the same spatial distribution as the stellar distribution assumed by Bailer-Jones et al. (2018), we must cautiously interpret the distances to LMXBs (Grimm, Gilfanov & Sunyaev 2002; see Section 3.1). For example, an exponential disc model would prefer smaller distances for objects along lines of sight that are out of the plane of the Milky Way. However, this may not be optimal for LMXBs, given that they can be displaced from the stellar distribution by supernova kicks. Of the matched XRBs, 76 of the Liu catalogue counterparts have a parallax: 24 of these counterparts are associated with LMXBs, while 52 are associated with HMXBs. As the GOF values in Tables 1 and 2 show, the astrometric goodness-of-fit is poor for many of these sources. The *Gaia* DR2 documentation suggests that $|\mathrm{GOF}| > 3$ indicates possible problems with the fit: 12 LMXBs and 44 HMXBs have values in this range. A large subset of sources in our sample (30) appear to show a large excess noise in their astrometric fit (larger than 5σ). A reason for the high GOF and large excess noise in these systems could be the orbital motion.

Several of the matched objects have a negative measured parallax. In this case, the distance we obtain is dominated by the assumptions of the prior (see discussion in Luri et al. 2018 and Hogg 2018). We plot the positions of the *Gaia* candidate counterparts to the XRBs for a face-on projection of the Milky Way in Figs 1 and 2.

3 RESULTS

Several expected results are evident in the Galactic distributions of the XRB sample. First, as shown in Fig. 1, HMXBs appear to trace out the nearby (i.e. within 5–8 kpc) arms of the Galaxy. Since HMXB luminosity is correlated with SFR in star-forming galaxies (Grimm et al. 2003; Mineo et al. 2012), and spiral arms are the primary sites of star formation, it is reasonable to infer that they should be spatially close to spiral arms. Fig. 2 shows that the LMXBs are preferentially found in the direction towards the Galactic Centre. A Rayleigh test rejects the null hypothesis that the Galactic longitudes of the LMXBs are uniformly distributed at $p = 1.5 \times 10^{-5}$ (and a Kuiper two-sample test rejects the hypothesis that the Galactic longitude distributions of the LMXBs and HMXBs are drawn from the same distribution at $p = 0.02$.) The concentration of LMXBs towards the Galactic Centre

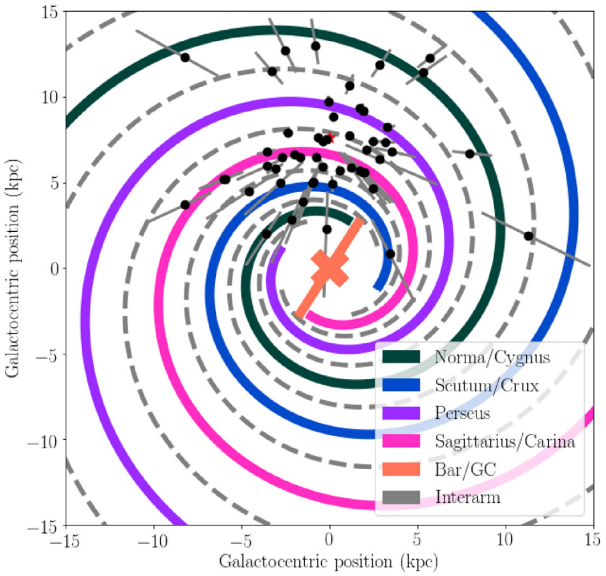

Figure 1. Face-on distribution of *Gaia* counterparts for Liu HMXBs. The spiral arms are modelled using the symmetric spiral arm model of Vallée (2008). Interarm regions are modelled as the symmetric arm model phase shifted by 45°. Error bars for distance/parallax represent the 1σ uncertainties. The sun is located at the red star in the middle upper portion of the Figure.

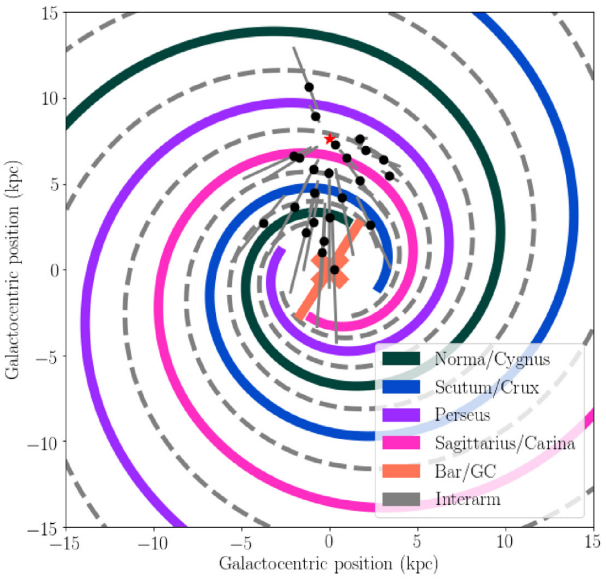

Figure 2. Face-on distribution of *Gaia* counterparts for Liu LMXBs. The spiral arms are modelled using the symmetric spiral arm model of Vallée (2008). Interarm regions are modelled as the symmetric arm model phase shifted by 45°. Error bars for distance/parallax represent the 1σ uncertainties. The sun is located at the red star in the middle upper portion of the Figure.

is also expected since LMXBs have been shown to trace stellar mass in galaxies (Gilfanov 2004) and are preferentially formed in dense areas with high stellar encounter rate, such as the Galactic Bulge (Muno et al. 2005; Degenaar et al. 2012).

3.1 Distance measurement comparison

We find *Gaia* parallax measurements for less than one-third of the combined LMXB/HMXB catalogue; in general, parallax

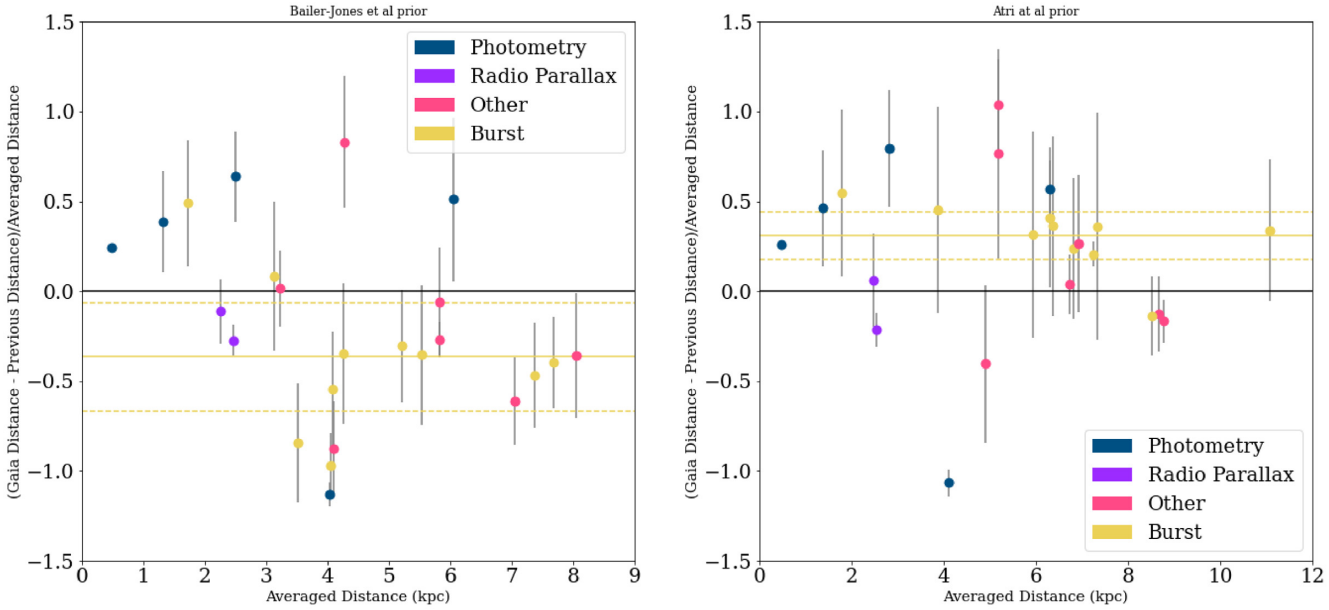

Figure 3. Difference between literature distance measurements for Liu catalogue LMXBs and the distances obtained in this work, versus the average of these distances. Error bars are lower limits because the uncertainties in the previous distance measurements were omitted. The horizontal yellow lines show the mean and 95 per cent confidence interval of the sources with previously measured distances using Type I X-ray burst. Left-hand panel: *Gaia* DR2 distances calculated using the prior of Bailer-Jones et al. (2018). Right-hand panel: *Gaia* DR2 distances calculated using the prior of Atri et al. (2019). Type I X-ray burst distances show a systematic overestimate with respect to the *Gaia* distances using the Bailer-Jones prior, and a systematic underestimate with respect to the *Gaia* distances that use the Atri et al. priors. The comparison using the prior of Bailer-Jones et al. (2018) implies that X-ray bursts (assuming they are PRE bursts) only reach 0.5 $L_{\rm Eddington}$.

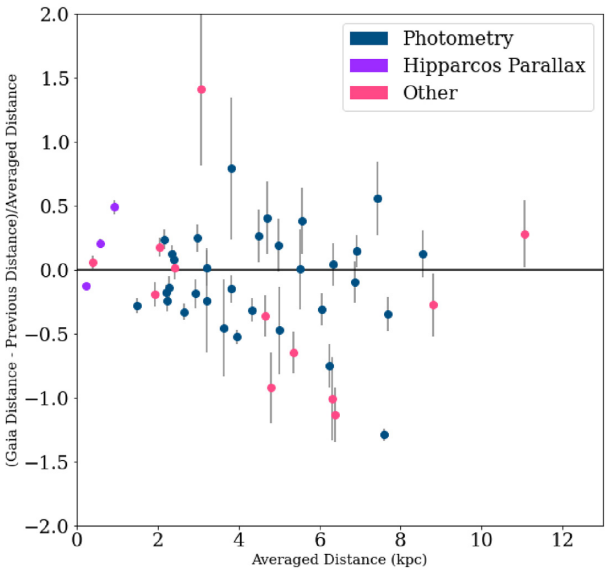

Figure 4. Difference between previous distance measurements for Liu catalogue HMXBs and the distances obtained in this work, versus the average of these distances. Previous distances are obtained from the literature reference given in Table 2, while the distance in this work is the distance to the *Gaia* candidate counterpart for each HMXB.

measurements will not be available for Galactic XRBs. Hence it is useful to use objects with parallax measurement as a diagnostic for other distance methods. We show a comparison of previous distance measurements with those derived from the *Gaia* candidate counterparts using Bland-Altman plots in Figs 3 and 4. These two figures show the ratio of the difference between previous measured distances and *Gaia* DR2 distances (this work) to the average of the measurements versus the average of the measurements. To estimate the error bars in these plots, we only used the uncertainties for our *Gaia* counterparts, but omit the uncertainties on previous measurements given the difficulties in comparing methods, instruments, and the fact that many distances are assumed rather than measured directly. A useful component of this work is to tabulate distance methods for XRBs with *Gaia* candidate counterparts, since in the Liu catalogue, distances are reported without specifying the methodology or whether distances are measured or assumed.

Most previous distance-measurement methods produce distances consistent with *Gaia*, within their uncertainties where available. *Gaia* DR2 measurements agree well with objects whose parallax has been previously measured either by *Hipparcos* or radio interferometery (VLBI/VLBA). Radio interferometery parallaxes are expected to be significantly more accurate than *Gaia*; therefore comparing with radio parallaxes verifies the assumptions of the *Gaia* prior, at least for the distance ranges and directions where objects with radio parallax are available. In addition, the mean and median differences between distances previously measured photometrically and *Gaia* DR2 distances are consistent with zero.

LMXB distances measured using Type I X-ray bursts do show evidence of a trend with a plausible physical interpretation. As shown in the left-hand panel of Fig. 3, distances measured using Type I X-ray bursts are systematically larger than those measured via *Gaia* candidate counterparts. This figure shows the ratio of difference between previously measured distance and *Gaia* distance to the average of previously measured distance and *Gaia* distance. The mean of this quantity over all the methods excluding the Type I X-ray bursts is -0.07 ± 0.32, consistent with the null hypothesis of no difference (zero mean) with a p-value of 0.17. However, the

Table 3. Statistical significance of previous distance measurements of LMXBs comparing to *Gaia* DR2 distances using Bailer-Jones priors.

Method	Mean	95 per cent CI	*p*-value
Burst	−0.36	[−0.66, −0.06]	0.01
Photometry	0.13	[−0.76, 1.02]	0.35
Radio parallax	−0.19	[−1.22, 0.84]	0.20
Other	−0.19	[−0.69, 0.31]	0.20

mean for the Type I X-ray bursts is -0.36 ± 0.29 with a *p*-value of 0.01, which means we can reject the null hypothesis of no systematic difference between measured distances from *Gaia* and distances from Type I X-ray bursts. The statistical significances of comparing other methods used in measuring LMXB distances with respect to *Gaia* distances are reported in Table 3. In this table, means and 95 per cent confidence intervals of differences are reported, and the *p*-values are calculated for the null hypothesis of zero means. According to this table, distances measured using Type I X-ray bursts are the only method that show a systematic difference with new measured distances in this work.

These results would seem to suggest that Type I X-ray bursts are intrinsically less luminous than predicted by modelling. This agrees with previous results on systematic biases in distance determination via Type I X-ray bursts. Galloway et al. (2008b) demonstrated that the choice to assume that the touchdown flux (the flux measured when the expanded photosphere of the NS touches down back on to its surface) is either at the Eddington luminosity or sub-Eddington may introduce large systematic uncertainties to distance measurements of X-ray bursting XRBs. Studies of bursting sources using the Rossi X-ray Timing Explorer have indicated that a number of these sources are significantly sub-Eddington in their peak fluxes (e.g. Galloway et al. 2008a).

As mentioned in Section 2.4, LMXBs do not follow the same spatial distribution as the stellar distribution assumed by Bailer-Jones et al. (2018). To investigate the effect of the priors on LMXB distances, we also measured the *Gaia* DR2 distances using the prior developed by Atri et al. (2019), which considers the distribution of LMXBs in the Milky Way based on the work of Grimm et al. (2002). The right-hand panel of Fig. 3 shows the result of our distance comparisons using this prior. The most noticeable effect of using the Atri et al. (2019) prior is an increase in distances for most of the LMXBs. As a result, distances measured using Type I X-ray bursts are systematically smaller than those measured via *Gaia* candidate counterparts. This is in contradiction with the suggestive results of our analysis using the Bailer-Jones et al. (2018) prior, which indicated that distances based on type I X-ray bursts are overestimated, and thus that bursts only reach 0.5 $L_{\rm Eddington}$. As a model-independent check, we have also done the same analysis without using any prior. In this scenario, the Type I X-ray burst distances are consistent with the null hypothesis of no difference with the *Gaia* distances, with a *p*-value of 0.19. This discrepancy highlights the importance of priors when using *Gaia* data for sources with large uncertainties.

Individual objects with particularly large discrepancies between previously published and *Gaia* candidate counterpart distances are discussed in Appendix B.

3.2 Spatial distribution and spiral arms

To investigate the relationship between XRBs and Galactic structure, we compare the XRB distributions to a model of the spiral arms of the Milky Way. Pettitt, Ragan & Smith (2020) show evidence for spiral structure traced by young stars, though it is not clear what the precise physical properties of the spiral structure are. Gorski & Barmby (2020) suggest a four arm spiral structure traced by maser-bearing evolved stars. We use the symmetric arm model of Vallée (2008). This model is analytically defined: the precise shape, symmetries, structure, and extent of the spiral arms of the Galaxy are non-trivial to determine due to our location within the Milky Way. This symmetric model is fitted to agree with a variety of observations, including dust, H I gas, CO gas, and maps of stellar velocities. This model defines the mid-point of four identical arms phase shifted by 90°. We further define the mid-point of interarm regions by shifting the existing arms by 45°.

For each XRB, we compute three properties:

(i) The two-dimensional distance to the nearest spiral arm for a face-on projection.
(ii) Whether the XRB is leading or trailing its closest spiral arm.
(iii) Whether the XRB is closer to the mid-point of a spiral arm or the mid-point of an interarm region.

Given that many of the uncertainties for the distances quite large, counts of these quantities depend strongly on the posterior distribution function of the distances. In order to assess how much these quantities change, we create 10 000 realizations of the distance for each object using the posterior distribution function defined in Bailer-Jones et al. (2018), and compute the three quantities above for each object in each iteration.

After computing whether each object is closer to an arm or interarm region, whether it is leading or trailing the nearest spiral arm, and the distance to the nearest spiral arm, we calculate the fraction of objects leading/trailing and fraction of objects close to an arm/interarm for each of the 10 000 runs. Under this construction, since we have effectively partitioned the Galaxy into two equally sized regions (closer to arm/closer to interarm, leading/trailing the nearest spiral arm), we expect the following for the distribution of these fractions: If the distribution of LMXBs/HMXBs fractions peaks at a value greater than 0.5 for a particular structure (arm/interarm/leading edge/trailing edge), then we interpret that LMXBs/HMXBs as being correlated with that structure. Conversely, if the distribution peaks at a value less than 0.5, we interpret LMXBs/HMXBs as being anticorrelated with that structure. If the distribution peaks at 0.5, we interpret LMXBs/HMXBs as being uncorrelated with that structure. We treat the uncorrelated case as the null hypothesis for LMXBs and HMXBs individually.

In each run, we exclude from the fraction any object that lies at a distance of less than 3.1 kpc from the Galactic Centre, classifying them separately as bulge sources. We choose 3.1 kpc because it is given as the half-length of the bar superimposed on the cartographic plots of Vallée (2008), and it is noted therein that it becomes difficult to separate the beginnings of the spiral arms from the bar itself at approximately this distance. In each run, on average two HMXBs and five LMXBs were classified as bulge sources. The resulting fractions and their uncertainty distributions are plotted in Fig. 5.

Across the simulation, LMXBs and HMXBs both appear to exhibit a roughly normal distribution in both fractions, though in both the leading/trailing or arm/interarm case, the LMXB distribution possesses a larger spread. To compare these measurements to each other and to the null hypothesis (that they are uncorrelated with arms/interarms and leading/trailing spiral arms), we tested these uncertainty distributions for normality. Since the interarm/trailing fraction is complementary to the arm/leading fraction, we consider only the arm/leading fractions. None of the four distributions is

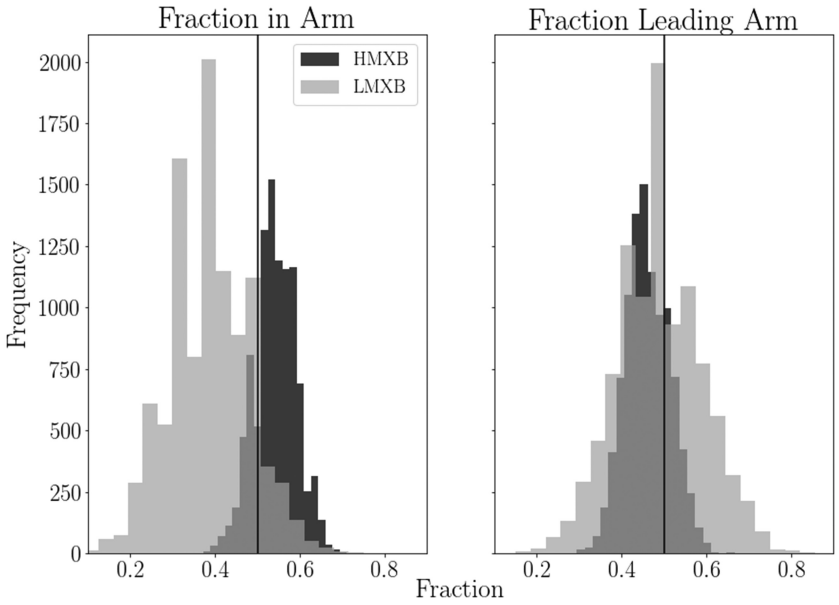

Figure 5. Distributions of population fraction correlated with spiral arms and leading edges for 10 000 realizations of the XRBs with *Gaia* candidate counterparts. The vertical line marks a fraction of 0.5, where the populations would be interpreted as being uncorrelated with the structure.

considered normal by the D'Agostini K^2 test or the Anderson–Darling test at $p = 0.05$. Only the LMXB leading fraction is considered normal by the Jarque-Bera test for $p = 0.05$. Since the distributions are not truly normal, we report the fraction measurements and their uncertainty in two ways: first using the standard deviation as the 1σ uncertainty, and then reporting the 95th/5th quantiles as the uncertainty.

Our measurements of the fraction of HMXBs/LMXBs that are correlated with spiral arms/interarm regions yields the following results:

(i) Fraction of HMXBs that are closer to a spiral arm: 0.54 ± 0.05 (at 1σ), $0.54^{+0.08}_{-0.08}$ at the 95th and 5th quantiles.
(ii) Fraction of LMXBs that are closer to a spiral arm: 0.39 ± 0.09 (at 1σ), $0.39^{+0.16}_{-0.15}$ at the 95th and 5th quantiles.
(iii) Fraction of HMXBs that are leading the nearest spiral arm: 0.46 ± 0.05 (at 1σ), $0.46^{+0.09}_{-0.09}$ at the 95th and 5th quantiles.
(iv) Fraction of LMXBs that are leading the nearest spiral arm: 0.50 ± 0.10 (at 1σ), $0.49^{+0.16}_{-0.17}$ at the 95th and 5th quantiles.

We cannot reject the null hypothesis that HMXBs or LMXBs are spatially uncorrelated with spiral arms, at even 1σ, since the uncertainties overlap with $F_{\rm fraction} = 0.5$. We cannot reject the null hypothesis for either HMXBs or LMXBs exhibiting no preference leading or trailing their nearest spiral arm. The LMXB and HMXB fractions also overlap with each other at the 1σ level. LMXBs exhibit a mild preference for being found in interarm regions, while HMXBs show only a mild preference for being found in the spiral arms. LMXBs appear to be uncorrelated with leading or trailing their spiral arm, while at low significance the HMXBs appear to prefer trailing their nearest spiral arm.

In the context of Galactic structure, previous work has shown that HMXBs trace SFR on Galactic scales (Grimm et al. 2003), so it is reasonable to expect they should trace it on resolved scales in some fashion and should exhibit a distinct spatial correlation. Naively it can be assumed that star formation should happen at the leading edge of a spiral arm where the gas accumulates (see Koda et al. 2012 for M51 as an illustrative example of star formation and its relation to spiral arm structure). Taking these assumptions together, HMXBs should be found at the leading edge of spiral arms, and should exhibit a strong preference for spiral arms versus interarm regions. However, we find only a mild preference for spiral arms: the distribution of fractions for the simulation peaks at 54 per cent of the HMXBs being closer to an arm than an interarm region, but the wings of the distribution include the uncorrelated and anticorrelated cases.

The lack of strong preference for HMXBs being closely associated with spiral arms could have a number of possible implications:

(i) Star formation does not occur at the leading edge of spiral arms.
(ii) The time delay between star formation and HMXB accretion starting manifests itself as a spatial separation between the spiral arm and HMXBs due to the pattern speed of spiral arms.
(iii) HMXB natal kicks may be larger than expected.
(iv) Our sample is not large enough and does not have sufficiently small distance uncertainties as an ensemble to measure the correlation we expect from first principles.

Our HMXB sample comprises only ∼50 objects, and the uncertainties are still substantial. As such, though we can rule out a very strong spatial correlation or anticorrelation between HMXBs and spiral arms (using the *Gaia* DR2 data specifically), we cannot use our result to distinguish between the scenarios listed above. Since we are unable to reject the null hypothesis that HMXBs are uncorrelated with spiral arms, our result is consistent with Bodaghee et al. (2012)'s analysis, which found that HMXBs are not spatially correlated with spiral arms. The scale at which the HMXB/SFR correlation breaks down (if at all) is not well constrained. In nearby galaxies, the X-ray sources are typically studied by considering the integrated properties of the entire population (for example, X-ray luminosity function) and comparing to global parameters of the Galaxy. Correlating XRBs with Galactic structure is challenging since galaxies that are close enough to resolve on the desired scales require many fields in order to encompass the entire Galaxy. In addition, contamination from X-ray sources in front of or behind the Galaxy creates additional difficulties. Swartz et al. (2003) investigated the relationship between

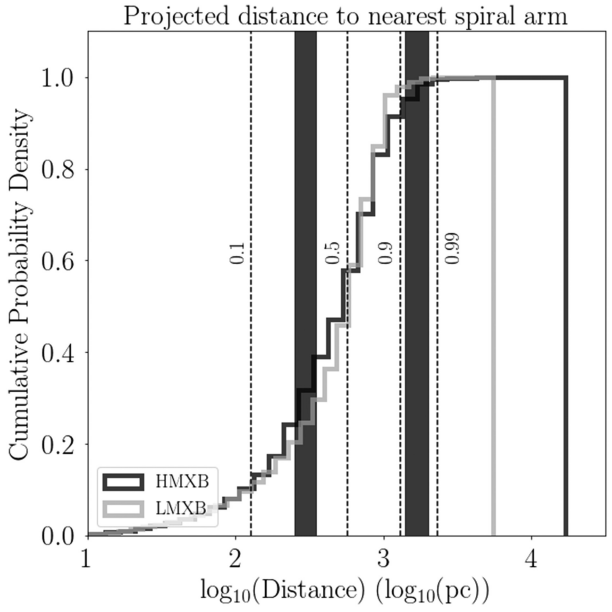

Figure 6. Cumulative distribution of XRB distances to the nearest spiral arm. We mark the characteristic clustering scales of HMXBs against OB associations and star-forming complexes measured by Bodaghee et al. (2012) and Coleiro & Chaty (2013) for reference using the vertical grey regions. We also plot the 0.1, 0.5, 0.9, and 0.99 quantiles of the HMXB distribution for comparison.

the spiral arms of M81 and its X-ray source population, finding strong correlation between spiral arm position and X-ray source density. They note that brighter sources tend to be closer to spiral arms, attributable to the brightest and shortest-lived HMXBs being close downstream from their spiral arms. More recently, Kuntz, Long & Kilgard (2016) performed a deep *Chandra* survey of M51. This study also finds that X-ray sources are concentrated in spiral arms, though the distances to spiral arm mid-points are not presented. Both studies also found a non-trivial population of supernova remnants contributing to the total X-ray source population.

In contrast to HMXBs, we expect that LMXBs should exhibit no strong preference for spiral arms; they represent (collectively) an older population that is also more strongly perturbed by the strength of its SN kicks (Grimm et al. 2002). Since LMXBs can be much older, it is not expected or required that they are still near the spiral arm that formed their progenitor – there may have been multiple Galactic rotations since the LMXB itself formed. Additionally, LMXBs' high velocity kicks mean they can be substantially displaced from the star-forming region where they initially formed. This process is already required to explain the presence of LMXBs at high Galactic latitudes where they would not be expected to form a priori due to the low stellar density (see e.g. Repetto et al. 2012). Consequently, LMXBs as a population should be uncorrelated with spiral arms since their distribution would be unperturbed by either the presence or absence of spiral arms. This makes our result, which shows LMXBs anticorrelated with spiral arms (though at low significance), difficult to explain.

We also computed the distribution of distances to the nearest spiral arm across all the simulations, shown in Fig. 6, in order to compare with previous works that measured the distances to OB associations and SFCs for HMXBs (Bodaghee et al. 2012; Coleiro & Chaty 2013). In these works, clustering distances between HMXBs and SFCs/OB associations were inferred from the critical points of the cumulative distribution of the distances to the nearest SFC/OB association. As discussed in Section 1.1, distances to OB associations and SFCs are distinct from distances to the spiral arms themselves, and as such we might not expect HMXBs to have the same clustering distance to the spiral arm. The distribution of HMXB distances to the nearest spiral arm that we measure does not show a strong preference for the clustering sizes measured for OB associations or SFCs in previous works, though we note that the Vallée (2008) model does not fit spiral arms to either of these structures. The 0.1, 0.5, 0.9, and 0.99 quantiles of the HMXB distribution to be at 127, 570, 1296, and 2340 pc, respectively. For the LMXB distribution, the 0.1, 0.5, 0.9, and 0.99 quantiles of the LMXB distribution are at 130, 610, 1090, and 1780 pc, respectively.

Given the substantial width of these distributions, it is difficult to determine a characteristic separation from the spiral arms. The interarm separation of a few kpc as set by the symmetric arms model means that, by construction, it is difficult to have an XRB more than a few kpc away from a spiral arm in face-on projection. Further, we have chosen to model the Galaxy using a symmetric model fitted to observables in the Milky Way, which is a simple albeit potentially unrealistic choice. The primary advantage of this model is that it permits us to easily define interarm and arm regions for analysis of the locations of XRBs. In reality, the number of arms and the symmetry (e.g. are the four arms symmetric with each other or are there major/minor axes?) of these arms in the Milky Way is difficult to characterize (see Vallée 2017 and references therein), and discussion exists about which tracers to use and how far to project the model based on nearby observables. Future attempts to characterize the relationship between the Galaxy's spiral arms and its XRB population would be improved by the use of a model that relaxes the symmetry constraint.

4 CONCLUSIONS

(i) We have assembled the largest sample of Galactic X-ray binaries whose distances have all been measured using the same method, and hence have the same systematics and uniform presumed biases.

(ii) Comparing XRB distances measured by *Gaia* (using the Bailer-Jones prior) to previous methods shows that measuring distances using Type I X-ray bursts appears to systematically overestimate distance. This suggests that assumptions about X-ray bursts, namely that bursting NSs consistently reach the Eddington luminosity, may need to be modified to use X-ray bursts as a distance estimator. This effect is prior dependent, as choosing a different prior, such as the one in Atri et al. (2019), can cause burst distances to be systematically lower than those from *Gaia* DR2.

(iii) We have compared the positions of XRBs to the locations of the mid-points of spiral arms in the Milky Way. Galactic HMXBs in our sample show only a modest preference for being spatially colocated with spiral arms versus interarm regions, and show only a modest preference for being on the leading edge of spiral arms. This suggests that the delay time between star formation and HMXB formation/accretion beginning manifests itself observationally as a spatial separation between HMXBs and spiral arms due to the pattern speed of spiral arm rotation. Other possible explanations for this effect are scattering due to natal HMXB kicks or the possibility of star formation occurring closer to the mid-point of the arm than the leading edge.

(iv) We further find that HMXB distances to the nearest spiral arm do not show a strong preference for the clustering sizes previously observed for OB associations or SFCs.

(v) We find that LMXBs are very weakly anticorrelated with spiral arms. This disagrees with the expectation that LMXBs should be uncorrelated with spiral arms, though we note that the significance of this result is low.

A main source of uncertainty in our analysis is the low number of XRBs with *Gaia* counterparts. Further releases of *Gaia* will hopefully yield additional *Gaia* candidate counterparts for Galactic XRBs, particularly for the intrinsically optically fainter LMXBs. For objects with identified *Gaia* candidate counterparts, smaller distance uncertainties are expected from the improved baseline in DR3 and subsequent releases. The small sample size from the Liu catalogues is another limitation of our analysis. The *Chandra* Source Catalog (Evans et al. 2010) provides an excellent foundation for studying the Galactic X-ray sky in the *Chandra* era, but at present it has not been data mined to make a Milky Way-specific catalogue as a potential successor to the Liu catalogues. Our knowledge of the Galactic XRB source population can be improved through future all-sky surveys, such as with the newly launched eROSITA mission (Merloni et al. 2012). This mission, designed as a successor to the *ROSAT* mission, will survey the sky at approximately 20 times the sensitivity of *ROSAT* in soft X-rays (0.5–2.0 keV), while providing the first imaging survey of the sky in hard X-rays (2–10 keV). The on-axis angular resolution of this telescope is expected to be comparable to that of *XMM–Newton*. An improved all-sky survey will allow us to find *Gaia* counterparts to an X-ray catalogue that is more up-to-date and is has more uniform systematics, enhancing our understanding of how XRB positions correlate with Galactic structure.

ACKNOWLEDGEMENTS

We thank the referee, P. Gandhi, for constructive and helpful reports. This work has made use of data from the European Space Agency (ESA) mission *Gaia* (https://www.cosmos.esa.int/gaia), processed by the *Gaia* Data Processing and Analysis Consortium (DPAC, https://www.cosmos.esa.int/web/gaia/dpac/consortium). Funding for the DPAC has been provided by national institutions, in particular the institutions participating in the *Gaia* Multilateral Agreement. RMA acknowledges support from a Natural Sciences and Engineering Research Council (NSERC) Canada Graduate Scholarship-Doctoral (CGS-D) scholarship. PB acknowledges support from an NSERC Discovery Grant and the hospitality of the Rotman Institute for Philosophy. We thank E. Cackett, S. Gallagher, and T.A.A. Sigut for helpful discussions.

DATA AVAILABILITY

The data underlying this article are available in the article and in its online supplementary material.

REFERENCES

Arenou F. et al., 2018, A&A, 616, A17
Atri P. et al., 2019, MNRAS, 489, 3116
Augusteijn T., van der Hooft F., de Jong J. A., van Kerkwijk M. H., van Paradijs J., 1998, A&A, 332, 561
Bahramian A., Heinke C. O., Degenaar N., Chomiuk L., Wijnands R., Strader J., Ho W. C. G., Pooley D., 2015, MNRAS, 452, 3475
Bailer-Jones C. A. L., Rybizki J., Fouesneau M., Mantelet G., Andrae R., 2018, AJ, 156, 58
Bamba A., Yokogawa J., Ueno M., Koyama K., Yamauchi S., 2001, PASJ, 53, 1179
Basinska E. M., Lewin W. H. G., Sztajno M., Cominsky L. R., Marshall F. J., 1984, ApJ, 281, 337
Bassa C. G., Jonker P. G., in't Zand J. J. M., Verbunt F., 2006, A&A, 446, L17
Baumgartner W. H., Tueller J., Markwardt C. B., Skinner G. K., Barthelmy S., Mushotzky R. F., Evans P. A., Gehrels N., 2013, ApJS, 207, 19
Belokurov V. et al., 2020, MNRAS, 496, 1922
Berghoefer T. W., Schmitt J. H. M. M., Cassinelli J. P., 1996, A&AS, 118, 481
Bhattacharyya S., 2010, Adv. Space Res., 45, 949
Blay P., Negueruela I., Reig P., Coe M. J., Corbet R. H. D., Fabregat J., Tarasov A. E., 2006, A&A, 446, 1095
Bodaghee A., Tomsick J. A., Rodriguez J., James J. B., 2012, ApJ, 744, 108
Boroson B., Kim D.-W., Fabbiano G., 2011, ApJ, 729, 12
Boubert D., Guillochon J., Hawkins K., Ginsburg I., Evans N. W., Strader J., 2018, MNRAS, 479, 2789
Bozzo E. et al., 2018, A&A, 613, A22
Bradshaw C. F., Fomalont E. B., Geldzahler B. J., 1999, ApJ, 512, L121
Brandt S., Castro-Tirado A. J., Lund N., Dremin V., Lapshov I., Syunyaev R., 1992, A&A, 262, L15
Brown A. G. A., Blaauw A., Hoogerwerf R., de Bruijne J. H. J., de Zeeuw P. T., 1999, in Lada C. J., Kylafis N. D., eds, The Origin of Stars and Planetary Systems, NATO Advanced Science Institutes (ASI) Series C Vol. 540, Kluwer Academic Publishers. p. 411
Butters O. W., Norton A. J., Mukai K., Tomsick J. A., 2011, A&A, 526, A77
Cadolle Bel M. et al., 2007, ApJ, 659, 549
Cantrell A. G. et al., 2010, ApJ, 710, 1127
Casares J., Jonker P. G., Israelian G., 2017, in Alsabti A. W., Murdin P., eds, Handbook of Supernovae. Springer International Publishing AG, Berlin, p. 1499
Casares J., Ribó M., Ribas I., Paredes J. M., Martí J., Herrero A., 2005, MNRAS, 364, 899
Chakrabarty D., Roche P., 1997, ApJ, 489, 254
Chan V. C., Bovy J., 2020, MNRAS, 493, 4367
Chernyakova M., Lutovinov A., Rodríguez J., Revnivtsev M., 2005, MNRAS, 364, 455
Chevalier C., Ilovaisky S. A., 1998, A&A, 330, 201
Clark G. W., 1975, ApJ, 199, L143
Clark G. W., 2004, ApJ, 610, 956
Coe M. J., Everall C., Norton A. J., Roche P., Unger S. J., Fabregat J., Reglero V., Grunsfeld J. M., 1993, MNRAS, 261, 599
Coe M. J. et al., 1994, MNRAS, 270, L57
Coleiro A., Chaty S., 2013, ApJ, 764, 185
Coley J. B., Corbet R. H. D., Krimm H. A., 2015, ApJ, 808, 140
Corbet R. H. D., Mason K. O., 1984, A&A, 131, 385
Corral-Santana J. M., Casares J., Muñoz-Darias T., Bauer F. E., Martínez-Pais I. G., Russell D. M., 2016, A&A, 587, A61
Cowley A. P., Schmidtke P. C., 1990, AJ, 99, 678
Dabringhausen J., Kroupa P., Pflamm-Altenburg J., Mieske S., 2012, ApJ, 747, 72
Degenaar N., Wijnands R., Cackett E. M., Homan J., in't Zand J. J. M., Kuulkers E., Maccarone T. J., van der Klis M., 2012, A&A, 545, A49
Dhawan V., Mirabel I. F., Ribó M., Rodrigues I., 2007, ApJ, 668, 430
Erkal D., Boubert D., Gualandris A., Evans N. W., Antonini F., 2019, MNRAS, 483, 2007
Evans I. N. et al., 2010, ApJS, 189, 37
Filliatre P., Chaty S., 2004, ApJ, 616, 469
Foellmi C., Depagne E., Dall T. H., Mirabel I. F., 2006, A&A, 457, 249
Foight D. R., Güver T., Özel F., Slane P. O., 2016, ApJ, 826, 66
Fortin F., Chaty S., Sander A., 2020, ApJ, 894, 86
Gaia Collaboration, 2016a, A&A, 595, A1
Gaia Collaboration, 2016b, A&A, 595, A2
Gaia Collaboration, 2018, A&A, 616, A1
Gaia Collaboration, 2020, A&A, in press, preprint (arXiv:2012.01533)
Galloway D. K., Muno M. P., Hartman J. M., Psaltis D., Chakrabarty D., 2008a, ApJS, 179, 360
Galloway D. K., Psaltis D., Chakrabarty D., Muno M. P., 2003, ApJ, 590, 999

Galloway D. K., Özel F., Psaltis D., 2008b, MNRAS, 387, 268
Gandhi P., Rao A., Johnson M. A. C., Paice J. A., Maccarone T. J., 2019, MNRAS, 485, 2642
Gelino D. M., 2001, PhD thesis, University of California
Gelino D. M., Harrison T. E., 2003, ApJ, 599, 1254
Gilfanov M., 2004, MNRAS, 349, 146
González Hernández J. I., Rebolo R., Peñarrubia J., Casares J., Israelian G., 2005, A&A, 435, 1185
Gorski M. D., Barmby P., 2020, MNRAS, 495, 726
Green G. M., Schlafly E., Zucker C., Speagle J. S., Finkbeiner D., 2019, ApJ, 887, 93
Grillo F., Sciortino S., Micela G., Vaiana G. S., Harnden F. R., 1992, ApJS, 81, 795
Grimm H.-J., Gilfanov M., Sunyaev R., 2002, A&A, 391, 923
Grimm H.-J., Gilfanov M., Sunyaev R., 2003, MNRAS, 339, 793
Grindlay J. E., Petro L. D., McClintock J. E., 1984, ApJ, 276, 621
Hakala P., Ramsay G., Muhli P., Charles P., Hannikainen D., Mukai K., Vilhu O., 2005, MNRAS, 356, 1133
Hjellming R. M., Johnston K. J., 1981, ApJ, 246, L141
Hjellming R. M., Rupen M. P., 1995, Nature, 375, 464
Hogg D. W., 2018, preprint (arXiv:1804.07766)
Hutchings J. B., Cowley A. P., Crampton D., van Paradijs J., White N. E., 1979, ApJ, 229, 1079
Ilovaisky S. A., Chevalier C., Motch C., 1982, A&A, 114, L7
in't Zand J. J. M., Cumming A., van der Sluys M. V., Verbunt F., Pols O. R., 2005, A&A, 441, 675
in't Zand J. J. M. et al., 2002, A&A, 389, L43
Janka H.-T., 2013, MNRAS, 434, 1355
Janot-Pacheco E., Ilovaisky S. A., Chevalier C., 1981, A&A, 99, 274
Jonker P. G., Galloway D. K., McClintock J. E., Buxton M., Garcia M., Murray S., 2004, MNRAS, 354, 666
Jonker P. G., Nelemans G., 2004, MNRAS, 354, 355
Kaaret P., Piraino S., Halpern J., Eracleous M., 1999, ApJ, 523, 197
Kaluzienski L. J., Holt S. S., Swank J. H., 1980, ApJ, 241, 779
Kawai N., Suzuki M., 2005, Astron. Telegram, 534, 1
Koda J. et al., 2012, ApJ, 761, 41
Krimm H. A. et al., 2013, ApJS, 209, 14
Krivonos R., Tsygankov S., Revnivtsev M., Grebenev S., Churazov E., Sunyaev R., 2010, A&A, 523, A61
Krzeminski W., 1974, ApJ, 192, L135
Kuntz K. D., Long K. S., Kilgard R. E., 2016, ApJ, 827, 46
Kuulkers E., den Hartog P. R., in't Zand J. J. M., Verbunt F. W. M., Harris W. E., Cocchi M., 2003, A&A, 399, 663
La Parola V., Cusumano G., Romano P., Segreto A., Vercellone S., Chincarini G., 2010, MNRAS, 405, L66
Leahy D. A., 2002, A&A, 391, 219
Lehmer B. D., Alexander D. M., Bauer F. E., Brandt W. N., Goulding A. D., Jenkins L. P., Ptak A., Roberts T. P., 2010, ApJ, 724, 559
Lewin W. H. G., van Paradijs J., Taam R. E., 1993, Space Sci. Rev., 62, 223
Linares M., Shahbaz T., Casares J., 2018, ApJ, 859, 54
Lin D., Webb N. A., Barret D., 2012, ApJ, 756, 27
Lindegren L. et al., 2018, A&A, 616, A2
Liu Q. Z., van Paradijs J., van den Heuvel E. P. J., 2006, A&A, 455, 1165
Liu Q. Z., van Paradijs J., van den Heuvel E. P. J., 2007, A&A, 469, 807
Luri X. et al., 2018, A&A, 616, A9
Lyuty V. M., Zaĭtseva G. V., 2000, Astron. Lett., 26, 9
MacDonald R. K. D. et al., 2014, ApJ, 784, 2
Marsden D., Gruber D. E., Heindl W. A., Pelling M. R., Rothschild R. E., 1998, ApJ, 502, L129
Masetti N., Orlandini M., Palazzi E., Amati L., Frontera F., 2006b, A&A, 453, 295
Masetti N. et al., 2002, A&A, 382, 104
Masetti N. et al., 2006a, A&A, 449, 1139
Masetti N. et al., 2006c, A&A, 455, 11
Masetti N. et al., 2009, A&A, 495, 121
Mason K. O., Cordova F. A., 1982, ApJ, 262, 253
Massey P., Johnson K. E., Degioia-Eastwood K., 1995, ApJ, 454, 151
McBride V. A. et al., 2006, A&A, 451, 267
McClintock J. E., Remillard R. A., Margon B., 1981, ApJ, 243, 900
Megier A., Strobel A., Galazutdinov G. A., Krełowski J., 2009, A&A, 507, 833
Merloni A. et al., 2012, preprint (arXiv:1209.3114)
Miller-Jones J. C. A., Jonker P. G., Dhawan V., Brisken W., Rupen M. P., Nelemans G., Gallo E., 2009, ApJ, 706, L230
Miller-Jones J. C. A. et al., 2021, Science, in press
Mineo S., Gilfanov M., Sunyaev R., 2012, MNRAS, 419, 2095
Motch C., Haberl F., Dennerl K., Pakull M., Janot-Pacheco E., 1997, A&A, 323, 853
Muno M. P., Chakrabarty D., Galloway D. K., Savov P., 2001, ApJ, 553, L157
Muno M. P., Pfahl E., Baganoff F. K., Brandt W. N., Ghez A., Lu J., Morris M. R., 2005, ApJ, 622, L113
Muñoz-Darias T., Casares J., Martínez-Pais I. G., 2005, ApJ, 635, 502
Negueruela I., Roche P., Buckley D. A. H., Chakrabarty D., Coe M. J., Fabregat J., Reig P., 1996, A&A, 315, 160
Negueruela I., Roche P., Fabregat J., Coe M. J., 1999, MNRAS, 307, 695
Negueruela I., Smith D. M., Harrison T. E., Torrejón J. M., 2006, ApJ, 638, 982
Nättilä J., Miller M. C., Steiner A. W., Kajava J. J. E., Suleimanov V. F., Poutanen J., 2017, A&A, 608, A31
Parkes G. E., Murdin P. G., Mason K. O., 1980, MNRAS, 190, 537
Pellizza L. J., Chaty S., Negueruela I., 2006, A&A, 455, 653
Perryman M. A. C. et al., 1997, A&A, 323, L49
Pettitt A. R., Ragan S. E., Smith M. C., 2020, MNRAS, 491, 2162
Phillips S. N., Shahbaz T., Podsiadlowski P., 1999, MNRAS, 304, 839
Podsiadlowski P., Rappaport S., 2000, ApJ, 529, 946
Polcaro V. F. et al., 1990, A&A, 231, 354
Pooley D. et al., 2003, ApJ, 591, L131
Prišegen M., 2019, A&A, 621, A37
Reid M. J., McClintock J. E., Narayan R., Gou L., Remillard R. A., Orosz J. A., 2011, ApJ, 742, 83
Reig P., Chakrabarty D., Coe M. J., Fabregat J., Negueruela I., Prince T. A., Roche P., Steele I. A., 1996, A&A, 311, 879
Reig P., Fabregat J., 2015, A&A, 574, A33
Reig P., Negueruela I., Papamastorakis G., Manousakis A., Kougentakis T., 2005, A&A, 440, 637
Reig P., Zezas A., Gkouvelis L., 2010, A&A, 522, A107
Repetto S., Davies M. B., Sigurdsson S., 2012, MNRAS, 425, 2799
Reynolds A. P., Bell S. A., Hilditch R. W., 1992, MNRAS, 256, 631
Reynolds A. P., Quaintrell H., Still M. D., Roche P., Chakrabarty D., Levine S. E., 1997, MNRAS, 288, 43
Sadakane K., Hirata R., Jugaku J., Kondo Y., Matsuoka M., Tanaka Y., Hammerschlag-Hensberge G., 1985, ApJ, 288, 284
Samus' N. N., Kazarovets E. V., Durlevich O. V., Kireeva N. N., Pastukhova E. N., 2017, Astron. Rep., 61, 80
Smith D. M., 2004, Astron. Telegram, 338, 1
Steele I. A., Negueruela I., Coe M. J., Roche P., 1998, MNRAS, 297, L5
Steiner A. W., Heinke C. O., Bogdanov S., Li C. K., Ho W. C. G., Bahramian A., Han S., 2018, MNRAS, 476, 421
Stevens J. B., Reig P., Coe M. J., Buckley D. A. H., Fabregat J., Steele I. A., 1997, MNRAS, 288, 988
Strohmayer T., Bildsten L., 2006, in Lewin W. H. G., van der Klis M., eds, Compact Stellar X-Ray Sources. Cambridge Astrophysics Series. Cambridge Univ. Press, Cambridge, p. 113
Swartz D. A., Ghosh K. K., McCollough M. L., Pannuti T. G., Tennant A. F., Wu K., 2003, ApJS, 144, 213
Tetarenko B. E., Sivakoff G. R., Heinke C. O., Gladstone J. C., 2016, ApJS, 222, 15
Thévenin F., Falanga M., Kuo C. Y., Pietrzyński G., Yamaguchi M., 2017, Space Sci. Rev., 212, 1787
Tomsick J. A., Gelino D. M., Kaaret P., 2005, ApJ, 635, 1233
Torrejón J. M., Negueruela I., Smith D. M., Harrison T. E., 2010, A&A, 510, A61
Torrejón J. M., Orr A., 2001, A&A, 377, 148
Tremmel M. et al., 2013, ApJ, 766, 19
Tsygankov S. S., Lutovinov A. A., 2005, Astron. Lett., 31, 88

Vallée J. P., 2008, AJ, 135, 1301
Vallée J. P., 2014, AJ, 148, 5
Vallée J. P., 2017, Astron. Rev., 13, 113
van Paradijs J., 1978, Nature, 274, 650
van Paradijs J., 1981, A&A, 101, 174
van Paradijs J., 1998, in Buccheri R., van Paradijs J., Alpar A., eds, NATO Advanced Science Institutes (ASI) Series C Vol. 515, Kluwer Academic Publishers, Dordrecht ; Boston. p. 279
van Paradijs J., White N., 1995, ApJ, 447, L33
Verbunt F., 2003, in Piotto G., Meylan G., Djorgovski S. G., Riello M., eds, ASP Conf. Ser. Vol. 296, New Horizons in Globular Cluster Astronomy. Astron. Soc. Pac., San Francisco, p. 245
Verbunt F., Hut P., 1987, in Helfand D. J., Huang J.-H., eds, Proc. IAU Symp. 125, The Origin and Evolution of Neutron Stars. Kluwer, Dordrecht, p. 187
Verbunt F., Lewin W. H. G., 2006, in Lewin W. H. G., van der Klis M., eds, Compact Stellar X-Ray Sources. Cambridge Astrophysics Series. Cambridge Univ. Press, Cambridge, p. 341
Verbunt F., van Paradijs J., Elson R., 1984, MNRAS, 210, 899
Wachter S., Smale A. P., 1998, ApJ, 496, L21
Wenger M. et al., 2000, A&AS, 143, 9
Wen L., Remillard R. A., Bradt H. V., 2000, ApJ, 532, 1119
Wilson C. A., Finger M. H., Coe M. J., Laycock S., Fabregat J., 2002, ApJ, 570, 287
Wilson C. A., Finger M. H., Coe M. J., Negueruela I., 2003, ApJ, 584, 996
Zhang Z., Gilfanov M., Bogdán Á., 2012, A&A, 546, A36

SUPPORTING INFORMATION

Supplementary data are available at *MNRAS* online.

Liu_catalog_non_matches

Please note: Oxford University Press is not responsible for the content or functionality of any supporting materials supplied by the authors. Any queries (other than missing material) should be directed to the corresponding author for the article.

APPENDIX A: UPDATED DISTANCES AND CLASSIFICATIONS OF XRBS WITH *Gaia* COUNTERPARTS

For the 88 *Gaia* candidate counterparts to the Liu XRB sample (see Section 2.3), we searched the literature for more recently published distances and compilations (Wenger et al. 2000; Corral-Santana et al. 2016; Tetarenko et al. 2016) for updates to classifications.

Two Liu catalogue objects have controversial classifications but do not figure in our analysis because their *Gaia* DR2 counterparts have no parallax. SIMBAD notes that the nature of 2S 0053+604 (γ Cas) as an X-ray binary is controversial (for a summary, see Prišegen 2019). Although the star itself is in *Gaia* DR2, its bright magnitude ($G = 1.82$) means that its observations require special processing expected in a later data release (Gaia Collaboration 2018). The object designated by Liu et al. (2006) as Swift J061223.0+701243.9 is claimed by SIMBAD to have incorrect nomenclature. As far as we can tell, this object is real and correctly designated by Liu but it is not particularly well studied, with no published distance estimate. The most recent analysis is by Butters et al. (2011) who conclude that Swift J061223.0+701243.9 is probably an intermediate polar, but an X-ray binary nature cannot be ruled out.

Six objects listed by Liu et al. (2006) as LMXBs are classified by SIMBAD as HMXBs. For three of these (1A 0620-00, GS 1124-684, GS 2023+338), the reference for the HMXB classification is Tetarenko et al. (2016); however, that catalogue does not give explicit LMXB/HMXB classifications. SIMBAD lists 3A 1516-569 (Cir X-1) and 3A 1954+319 as being classified as LMXBs by Baumgartner et al. (2013) and as HMXBs by Samus' et al. (2017) and Krivonos et al. (2010), respectively. Neither of the latter two sources gives a reference or justification for the HMXB classification. SIMBAD lists GRO J1655-40 as being classified as HMXB by Lin, Webb & Barret (2012) and LMXB by Krimm et al. (2013). However, Lin et al. (2012) did not classify sources as high- or low-mass XRBs, and the classifications in Krimm et al. (2013) are cited as originating from the literature or SIMBAD itself. With no strong reasons to reclassify these six objects, we retain them in our list of LMXBs.

Table A1. XRBs with *Gaia* candidate counterparts and newer published distances.

Name	Liu dist. (kpc)	Type	$d_{\rm prev}$ (newer) (kpc)	Type
LMXBs				
GRO J0422+32	···	···	2.49	SEDfit
1A 0620-00	1.16	phot	1.06	phot
GS 1124-684	5.5	phot	5.9	SEDfit
3A 1516-569	···	···	9.2	burst
GRO J1655-40	1.7	phot	3.2	jetPM
3A 1702-363	···	···	9.2	unclear
4U 1724-307	7	burst	9.5	cluster
SLX 1737-282	7.5	burst	6.5	burst
4U 1908+005	5	Roche	5.2	burst
HMXBs				
IGR J01583+6713	···	···	6.4	phot
EXO 051910+3737.7	···	···	1.7	phot
IGR J06074+2205	···	···	4.5	phot
XTE J0658-073	···	···	3.9	phot
IGR J11215−5952	8	phot	6.2	phot
IGR J11435−6109	···	···	8.6	phot
2S 1145-619	2.25	phot	3.1	phot
4U 1223-624	5	phot	4.1	phot
1H 1249-637	0.3	HipPLX	0.392	Av
IGR J16479−4514	···	···	4.45	phot
4U 1700-37	1.9	phot	2.12	Av
IGR J17544−2619	10	unknown	3.2	phot
SAX J1819.3−2525	6	SEDfit	6.2	SEDfit
IGR J19140+0951	···	···	3.6	phot
KS 1947+300	10	phot	9.5	pulsar
4U 1956+35	2.14	cluster	1.86	VLBAPLX

Note. 'Newer' here means non-*Gaia* DR2 distances published after the Liu et al. catalogues.

We were able to find published distance estimates for 10 objects that had no distance estimates listed by Liu et al. (2006, 2007). 15 additional objects in our sample had distance determinations more recent than those listed by Liu et al. (2006, 2007). We tabulate these in Table A1 and use them in our analysis in Section 3.1.

Two objects in our sample have controversial distances: Cyg X-1 and GRO J1655-40. The discrepancy between radio parallax distance (from Reid et al. 2011) and optical parallax from *Gaia* of Cyg X-1 is peculiar, as this system is one of the closest and brightest X-ray binaries (both in radio and optical). This apparent tension is likely caused by impact of the radio jet on the radio parallax (Miller-Jones et al. 2021). The *Gaia* distance is more consistent with that reported in the Liu catalogue (2.14 kpc; Massey, Johnson & Degioia-Eastwood 1995). Foellmi et al. (2006) challenged the accepted distance to GRO J1655-40 of 3.2 kpc, finding a distance of 1.7 kpc. Despite their strong claim, these authors show in their table 1 that the uncertainty in spectral class allows the upper limit on distance to be as high as 3–4 kpc (e.g. if the companion is F7ii). Interestingly, the *Gaia* counterpart parallax is consistent with the larger distance.

However, the location of the source makes distance calculation based on parallax strongly dependent on the prior model: there is a large discrepancy between the distance based on Bailer-Jones prior ($\sim$3 kpc) and one that considers distribution of BHs in the Milky Way ($\sim 6 - 7$ kpc), as shown by Atri et al. (2019).

APPENDIX B: DISTANCE DISCREPANCIES

In this section, we discuss five objects with large discrepancies between distances gathered from the literature and measured from *Gaia* DR2 with the Bailer-Jones et al. (2018) prior. Here we define 'large' as $|d_{\rm Gaia} - d_{\rm prev}|/(0.5 \times (d_{\rm Gaia} + d_{\rm prev})) > 1$. For all of these objects, the previously published distance is well outside the *Gaia* low-to-high range. We report the *Gaia* DR2 `astrometric_gof_al` value as GOF. This quantity is expected to follow a normal distribution with zero mean and unit standard deviation; hence absolute values $\gtrsim$3 indicate a poor fit.

4U 2129+47/V1727 Cyg: *Gaia* distance 1.75 kpc, GOF 1.92. The Liu et al. (2007) distance for this object is from the work of Cowley & Schmidtke (1990), who derive a distance of 6.3 kpc to the optical companion. Those authors mention that it is unclear that the companion and XRB are a true physical association, and that previous distance estimates to the XRB system generally give smaller distances (e.g. 2.2 kpc; McClintock, Remillard & Margon 1981). We conclude that the *Gaia* distance is consistent with these earlier estimates.

IGR J16318−4848: *Gaia* distance 5.22 kpc, GOF 32.4. The Liu et al. (2006) distance for this object is from the work of Filliatre & Chaty (2004) who give a range of distances between 0.9 and 6.2 kpc, derived from SED fitting. A more recent work (Fortin, Chaty & Sander 2020) determines a distance from *Gaia* matching and derives the same distance as our work. We conclude that the *Gaia* distance, although imprecise, is consistent with the broad range in the previous estimate.

IGR J16465−4507: *Gaia* distance 2.70 kpc, GOF 9.0. The Liu et al. (2006) distance for this object is from the work of Smith (2004) who give an estimated distance of 12.5 kpc based on photometry of the companion. The discussion of this object by La Parola et al. (2010) explains that the optical companion is highly absorbed; optical spectroscopic studies also provide additional evidence reaffirming the optical counterpart. The tension between the *Gaia* and previous distance estimates remains unresolved.

XTE J1906+09: *Gaia* distance 2.77 kpc, GOF 6.8. The Liu et al. (2006) distance for this object is from the work of Marsden et al. (1998) who give an estimate distance of 10 kpc based on neutral hydrogen absorption. However, 3D dust maps in this directions (Green et al. 2019) indicate that $E(g - r) \leq 2.2$, which would suggest that the Galactic hydrogen column density in this direction is $\leq 2 \times 10^{22}$ cm^{-2} (Bahramian et al. 2015; Foight et al. 2016). Thus we conclude that the *Gaia* distance is likely more reliable for this object.

KS 1947+300: *Gaia* distance 3.1 kpc, GOF 0.0. The Liu et al. (2006) distance for this object is from the work of Tsygankov & Lutovinov (2005) who give an estimate distance of 9.5 kpc based on its X-ray pulsation properties. While the *Gaia* fit appears good, it is important to note that the measured parallax is insignificant when uncertainties are considered.

This paper has been typeset from a TEX/LATEX file prepared by the author.